Distributed Zero-Forcing Amplify-and-Forward Beamforming for WSN Operation in Interfered and Highly Scattered Environments

Slim Zaidi, Oussama Ben Smida, Sofiène Affes, *Senior Member, IEEE*, and Shahrokh Valaee

***Abstract*— In this paper, amplify-and-forward beamforming (AFB) is considered to establish a communication, through wireless sensor networks (WSNs) of K sensor nodes, from a source to a receiver in the presence of both scattering and interference. All sources send their data to the WSN during the first time slot, while the nodes forward a properly weighted version of their received signals during the second slot. These weights are properly selected to maximize the desired power while completely canceling the interference signals. We show, however, that they depend on information locally unavailable at each node, making the zero-forcing beamformer (ZFB) unsuitable for WSNs, due to the prohibitive data exchange overhead and the power depletion it would require. To address this issue, we exploit the asymptotic expression at large K of the ZFB weights that is locally computable at every node and, further, well-approximates their original counterparts. The performance of the resulting new distributed ZFB (DZFB) version is analyzed and compared with the conventional ZFB and two other distributed AFB benchmarks: the monochromatic (i.e., single-ray) AFB whose design neglects the presence of scattering and the bichromatic AFB which relies on an efficient two-ray channel approximation valid only for low angular spread (AS). We show that the proposed DZFB outperforms its monochromatic and bichromate counterparts while incurring much less overhead and power depletion than ZFB. We show also that it is able to provide optimal performance even in highly scattered environments as in the latter.**

***Index Terms*— Amplify-and-forward (AF) beamforming (AFB), wireless sensor networks (WSN), scattering, beampattern, cost and power efficiencies, overhead.**

I. Introduction

THE potential of beamforming to improve the communication range and reliability and the energy efficiency of wireless sensor networks (WSNs) is now well understood in the literature [1]–[4]. Using this technique, a communication link between distant transceivers is established through K WSN nodes that simultaneously transmit weighted versions of their received signals. These amplify-and-forward (AF) beamforming (AFB) weights are properly designed to ensure a constructive combination at the desired direction of the nodes' radiated energies. When the total transmit power is fixed, AFB can achieve up to K-fold gain in the received power at the intended direction [9], [13], [15]. As such, not only the communication range is substantially extended, but also each node decreases its transmission power inversely proportional to K, thereby preserving their limited energy resources.

The AFB has aroused an increased interest due to its practical benefits. Reference [2] has introduced the AFB concept and analyzed the behavior of its beampattern when nodes are uniformly distributed. Beampattern characteristics have been also evaluated in [4] when the nodes are Gaussian distributed. Reference [5] analyzed the beampattern properties for several node distributions, [6] and [8] have, respectively, proposed nodes selection schemes aiming to achieve narrower mainbeam and minimum sidelobe effects. [9] has studied the robustness of AFB against the nodes asynchrony and [10] has proposed synchronization methods suitable for WSNs. References [12] and [13] have summarized the different beamforming techniques and their required synchronization approaches, respectively.

Despite their valuable contributions, all these works assume single-ray (i.e., monochromatic) channels that are very often invalid in real-world applications due to the presence of scattering. Characterized by its angular spread (AS), such a phenomenon replicates the transmit signal along multiple rays from different angles, thereby forming a multi-ray (i.e., polychromatic) channel [16]–[24]. Reference [21] has studied the scattering effect on monochromatic AFB whose design neglects such a phenomenon to show that its performance significantly deteriorates when AS increases. Aiming to address this issue, [22] and [23] have developed bichromatic AFBs which rely on an efficient two-ray channel approximation valid only for low AS. It has been shown that their performances are almost optimal in lightly- to moderately-scattered environments where AS is small. However, they deteriorate in highly-scattered environments where AS is large, more so in the presence of interference.

Manuscript received April 11, 2018; revised October 24, 2018 and January 30, 2019; accepted March 13, 2019. Date of publication March 20, 2019; date of current version February 14, 2020. This work was supported by the NSERC/Huawei Canada/TELUS CRD Grant on 5G-WAVES (Wireless Access Virtualization Enabling Schemes), the DG and CREATE PERSWADE Programs of NSERC, a Discovery Accelerator Supplement Award from NSERC, and the Cyrille-Duquet Research Chair in Telecommunications. The associate editor coordinating the review of this article and approving it for publication was T. Kim. *(Corresponding author: Slim Zaidi.)*

S. Zaidi and S. Valaee are with the ECE Department, University of Toronto, Toronto, ON M5S 3G4, Canada (e-mail: slim.zaidi@utoronto.ca; valaee@utoronto.ca).

O. Ben Smida and S. Affes are with the EMT Centre, Montreal, QC H5A 1K6, Canada (e-mail: oussama.ben.smida@emt.inrs.ca; affes@emt.inrs.ca).

Digital Object Identifier 10.1109/TCOMM.2019.2906609

In order to cope with real-world conditions, many works adopted under different expressions "optimal"[1] amplify-and-forward beamforming (OB) since it is the sole design able to properly handle both interference and scattering [22]–[30]. Unfortunately, each OB weight depends not only on the node's channel state information (CSI)s, but also on the other nodes' CSIs. Since WSN nodes are autonomous and, hence, do not a priori have access to the other nodes' CSIs, they have to exchange the latter to be able to compute their respective weights. This results in both huge data overhead and node power depletion, making OB unsuitable for WSNs. This critical impediment motivates us to design a new AFB technique able to approach OB performance at very low overhead and power costs.

In this paper, OB is considered to establish a communication through a WSN of K sensor nodes from a source to a receiver in the presence of both scattering and interference. All sources send their data to the WSN during the first time slot while the nodes forward a properly weighted version of their received signals during the second slot. These zero-forcing beamforming (ZFB) weights are properly selected to maximize the desired power while completely canceling the interference signals. We show, however, that they depend on information locally unavailable at each node, making them unsuitable for WSNs from the prohibitive data exchange overhead and power depletion they would otherwise require. To address this issue, we exploit the asymptotic expression at large K of the ZFB weights that is locally computable at every node and, further, well-approximates their original counterparts. The performance of the resulting new distributed ZFB (DZFB) version is analyzed and compared to ZFB and both monochromatic and bichromatic AFBs to highlight its significant performance advantages over all benchmarks.

Notation: Uppercase and lowercase bold letters denote matrices and column vectors, respectively. $[\cdot]_{il}$ and $[\cdot]_i$ are the (i,l)-th entry of a matrix and i-th entry of a vector, respectively. $(\cdot)^*$, $(\cdot)^T$, and $(\cdot)^H$ denote the complex conjugate, the transpose, and the Hermitian transpose, respectively. $\|\cdot\|$ is the 2-norm of a vector, $|\cdot|$ is the absolute value, and $\odot$ is the element-wise product. $J_n(\cdot)$ and $I_n(\cdot)$ stand for the first-kind Bessel function and the modified Bessel function of order n, respectively.

II. System Model

As illustrated in Fig. 1, we consider a WSN of K sensor nodes, each equipped with a single antenna, a receiver Rx, and M sources including a desired source and $M_I = M-1$ interfering ones. The nodes are assumed to be uniformly distributed over a disc of radius R. It is also assumed that the channel from the desired source to the destination experiences severe pathloss attenuation making the latter unable to communicate directly, i.e., without relaying from the K sensor nodes. Let (A_m, ϕ_m) and (r_k, ψ_k) denote the polar coordinates of the m-th source and the k-th node, respectively. Without any loss of generality, $(A_1, \phi_1 = 0)$ is assumed to be the location of the desired source. We also assume that the m-th source is located in the far-field region and, hence, $A_m \gg R$.

[1]In the sense that they assume perfect knowledge of both the desired and interfering channels or some quantized approximations thereof.

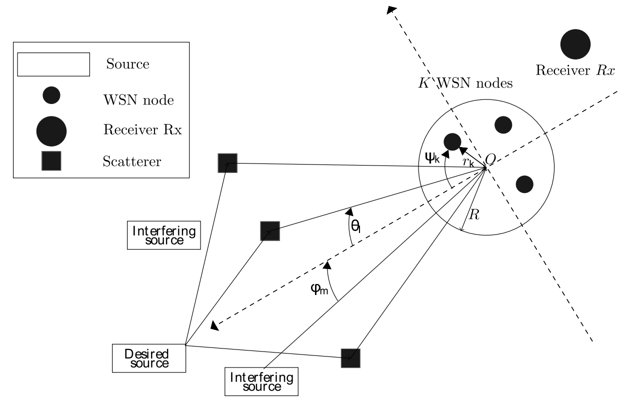

Fig. 1. System model.

The following assumptions are also adopted in this work:

(i) Due to the presence of a given number of scatterers, L_m rays are generated from the m-th source signal to form a polychromatic channel. The l-th ray has a complex amplitude $\alpha_{l,m}$ and an angle deviation $\theta_{l,m}$ from the nominal direction ϕ_m. The $\alpha_{l,m}$s are independent and identically distributed (i.i.d) zero-mean random variables (RV)s with variance $1/L_m$. The $\theta_{l,m}$s are i.i.d. zero-mean RV with a symmetric probability density function (pdf) $p_m(\theta)$ and variance σ_m^2. The latters are known as scattering distribution and angular spread (AS), respectively. All $\theta_{l,m}$s and $\alpha_{l,m}$s are mutually independent.

(ii) The k-th node's forward channel (i.e., from this node to the receiver) $[\mathbf{f}]_k$ is a circular complex Gaussian zero-mean RV with unit-variance and, hence, its magnitude follows a Rayleigh distribution whose parameter $\frac{1}{\sqrt{2}}$.

(iii) Noises at both the receiver and nodes are zero-mean Gaussian RVs with variances σ_n^2 and σ_v^2, respectively. All sources' signals are narrow band zero-mean RVs statistically independent from noises and channels.

(iv) Each node has perfect knowledge of its own location and forward channel, the wavelength λ, and the total number of WSN nodes K. However, it is not privy to other nodes information (i.e., locations and channels).

Note that (i), which is frequently adopted in the context of scattering environments, is due to both the sources' far-field location and the presence of scatterers [19]–[24]. In such a case, channels experience large-scale fading where the pathloss and scattering phenomenon are predominant. In turns, (ii) is due to the short distance between Rx and nodes, making their channels experience small scale-fading often modeled as Rayleigh distribution [15], [29], [31], [32].

Assumption (i) along with $A_m \gg R$ implies that the backward channel $[\mathbf{g}_m]_k$ from the m-th source to the k-th node is

$$[\mathbf{g}_m]_k = \sum_{l=1}^{L_m} \alpha_{l,m} e^{-j\frac{2\pi}{\lambda} r_k \cos(\phi_m + \theta_{l,m} - \psi_k)}. \tag{1}$$

Please note that (1) generalizes the well-known steering vector in the array-processing literature [2]–[6], [16], [23]. Indeed, (1) reduces to

$$\left[\mathbf{g}_m^{(1)}\right]_k = e^{-j(2\pi/\lambda) r_k \cos(\phi_m - \psi_k)}, \tag{2}$$

in scattering-free environments where $\sigma_m = 0$. Please note that $\left[\mathbf{g}_m^{(1)}\right]_k$ is the monochromatic single-ray channel adopted when designing the monochromatic AFB (MB) technique.

III. Zero-Forcing AF Beamformer

The desired source communicates with Rx over a dual-hop transmission. The m-th source also sends its signal s_m to the WSN during the first time slot. The received signal vector $\mathbf{y}$ at the WSN nodes is

$$\mathbf{y} = \mathbf{g}_1 s_1 + \mathbf{G}_\mathrm{I}\mathbf{s}_\mathrm{I} + \mathbf{v}, \tag{3}$$

where $\mathbf{G}_\mathrm{I} = [\mathbf{g}_2 \ldots \mathbf{g}_M]$, $\mathbf{s}_\mathrm{I} = [s_2 \ldots s_M]^T$, and $\mathbf{v}$ denotes the noise vector at the nodes. During the second time slot, the k-th node forwards its received signal after multiplying it with the complex conjugate of the beamforming weight w_k. Hence, Rx receives

$$\begin{aligned} r &= \mathbf{f}^T\left(\mathbf{w}^* \odot \mathbf{y}\right) + n \\ &= \mathbf{w}^H\left(\mathbf{f} \odot \left(\mathbf{g}_1 s_1 + \mathbf{G}_\mathrm{I}\mathbf{s}_\mathrm{I}\right) + \mathbf{f} \odot \mathbf{v}\right) + n \\ &= s_1 \mathbf{w}^H \mathbf{h}_1 + \mathbf{w}^H \mathbf{H}_\mathrm{I}\mathbf{s}_\mathrm{I} + \mathbf{w}^H\left(\mathbf{f} \odot \mathbf{v}\right) + n, \end{aligned} \tag{4}$$

where n is the receiver's noise, $\mathbf{h}_1 = \mathbf{f} \odot \mathbf{g}_1$, and $\mathbf{H}_\mathrm{I} = [\mathbf{f} \odot \mathbf{g}_2 \ldots \mathbf{f} \odot \mathbf{g}_M]$ is a matrix of dimension (K, M_I). Various design approaches may be adopted to derive the beamforming weights. Among them is the zero-forcing (ZF) approach that puts nulls at the interfering directions while ensuring a unit response at the desired source direction. Mathematically, the ZF beamforming (ZFB) vector $\mathbf{w}_\mathrm{ZF}$ must satisfy the following equations:

$$\mathbf{w}_\mathrm{ZF}^H \mathbf{H}_\mathrm{I} = 0, \tag{5}$$

$$\mathbf{w}_\mathrm{ZF}^H \mathbf{h}_1 = 1. \tag{6}$$

It can be easily shown that $\mathbf{w}_\mathrm{ZF}$ is given by

$$\mathbf{w}_\mathrm{ZF} = \frac{\left(\mathbf{h}_1 - \mathbf{H}_\mathrm{I}\left(\mathbf{H}_\mathrm{I}^H\mathbf{H}_\mathrm{I}\right)^{-1}\mathbf{H}_\mathrm{I}^H\mathbf{h}_1\right)}{\left(\|\mathbf{h}_1\|^2 - \mathbf{h}_1^H\mathbf{H}_\mathrm{I}\left(\mathbf{H}_\mathrm{I}^H\mathbf{H}_\mathrm{I}\right)^{-1}\mathbf{H}_\mathrm{I}^H\mathbf{h}_1\right)}. \tag{7}$$

Please note in order to derive $\mathbf{w}_\mathrm{ZF}$, one need to compute the inverse of $\mathbf{H}_\mathrm{I}$ [12]. Since K is typically much larger than M_I especially in WSN applications, $\mathbf{H}_\mathrm{I}$ is not a square matrix and, hence, its inverse does not exist. Nevertheless, according to its definition, $\mathbf{H}_\mathrm{I}$ has linearly independent columns, making thereby the square matrix $\left(\mathbf{H}_\mathrm{I}^H\mathbf{H}_\mathrm{I}\right)$ invertible. Consequently, one may resort to the pseudo inverse $\left(\mathbf{H}_\mathrm{I}^H\mathbf{H}_\mathrm{I}\right)^{-1}\mathbf{H}_\mathrm{I}^H$ as in 7.

In order to implement $\mathbf{w}_\mathrm{ZF}$, the k-th node must then be able to compute its corresponding weight

$$[\mathbf{w}_\mathrm{ZF}]_k = \left([\mathbf{h}_1]_k - \sum_{m=1}^{M}[\mathbf{H}_\mathrm{I}]_{km}\left[\left(\mathbf{H}_\mathrm{I}\mathbf{H}_\mathrm{I}^H\right)^{-1}\mathbf{H}_\mathrm{I}^H\mathbf{h}_1\right]_m\right) \times\left(\sum_{k=1}^{K}\left(|[\mathbf{h}_1]_k|^2 - [\mathbf{h}_1]_k\sum_{m=1}^{M}[\mathbf{H}_\mathrm{I}]_{km}\left[\left(\mathbf{H}_\mathrm{I}\mathbf{H}_\mathrm{I}^H\right)^{-1}\mathbf{H}_\mathrm{I}^H\mathbf{h}_1\right]_m\right)\right)^{-1}. \tag{8}$$

A straightforward inspection of (8) reveals that $[\mathbf{w}_\mathrm{ZF}]_k$ depends not only on $[\mathbf{h}_1]_k$, $k = 1, \ldots, K$, but also $\left[\left(\mathbf{H}_\mathrm{I}\mathbf{H}_\mathrm{I}^H\right)^{-1}\mathbf{H}_\mathrm{I}^H\mathbf{h}_1\right]_m$, $m = 2, \ldots, M$ both dependent on the coordinates and channels of all collaborating WSN nodes. As the latters are completely independent and autonomous, they would need to exchange their locally available information with each other in order to compute their weights, thereby resulting in a prohibitive overhead that can hinder both WSN spectral and power efficiencies. Consequently, the conventional ZFB in (7) is unsuitable for implementation in WSNs.

IV. Proposed AF Beamformer

To address the aforementioned critical issue, we propose in this work to substitute $\left(\mathbf{H}_\mathrm{I}^H\mathbf{H}_\mathrm{I}\right)^{-1}\mathbf{H}_\mathrm{I}^H\mathbf{h}_1$ and $\|\mathbf{h}_1\|^2/K$ in $\mathbf{w}_\mathrm{ZF}$ with their asymptotic approximations at large K given as

$$\begin{aligned} \lim_{K\to\infty}\left(\mathbf{H}_\mathrm{I}^H\mathbf{H}_\mathrm{I}\right)^{-1}\mathbf{H}_\mathrm{I}^H\mathbf{h}_1 &= \left(\lim_{K\to\infty}\frac{\mathbf{H}_\mathrm{I}^H\mathbf{H}_\mathrm{I}}{K}\right)^{-1}\lim_{K\to\infty}\frac{\mathbf{H}_\mathrm{I}^H\mathbf{h}_1}{K} \\ &= \mathbf{\Pi}^{-1}\boldsymbol{\beta}, \end{aligned} \tag{9}$$

and

$$\lim_{K\to\infty}\frac{\left\|\mathbf{h}_1^2\right\|}{K} = \boldsymbol{\beta}_0, \tag{10}$$

respectively. Actually, this approximation is motivated by the fact that the number of WSN nodes is typically large. In what follows, we will prove that both $\mathbf{\Pi}$ and $\boldsymbol{\beta}$ depend on the information locally available at each node, thereby paving the way towards the distributed implementation of ZFB in such networks. Let us first start by $\mathbf{\Pi}$. According to the definition of $\mathbf{H}_\mathrm{I}$, we have for $p, q = 1, \ldots, M_I$

$$\begin{aligned} [\mathbf{\Pi}]_{pq} &= \lim_{K\to\infty}\frac{1}{K}\left[\mathbf{H}_\mathrm{I}^H\mathbf{H}_\mathrm{I}\right]_{pq} \\ &= \sum_{l,l'=1}^{L}\alpha_{l,p+1}\alpha_{l',q+1}^*\lim_{K\to\infty}\sum_{k=1}^{K}\frac{|[\mathbf{f}]_k|^2}{K} \\ &\quad\times e^{-j\frac{2\pi}{\lambda}r_k\left(\cos(\phi_{q+1}+\theta_{l,p+1}-\psi_k)-\cos\left(\phi_{p+1}+\theta_{l',q+1}-\psi_k\right)\right)}. \end{aligned} \tag{11}$$

Exploiting the strong law of large numbers (LLN), we obtain

$$\begin{aligned} [\mathbf{\Pi}]_{pq} = \sum_{l,l'=1}^{L}\alpha_{l,p+1}\alpha_{l',q+1}^*\mathrm{E}_{r_k,\psi_k,[\mathbf{f}]_k}\Bigg\{&|[\mathbf{f}]_k|^2 \\ &\times e^{-j\frac{2\pi}{\lambda}r_k\left(\cos(\phi_{q+1}+\theta_{l,p+1}-\psi_k)-\cos\left(\phi_{p+1}+\theta_{l',q+1}-\psi_k\right)\right)}\Bigg\}, \end{aligned} \tag{12}$$

where $\mathrm{E}_{r_k,\psi_k,[\mathbf{f}]_k}$ stands for the expectation taken with respect to the random variables r_ks, ψ_ks, $[\mathbf{f}]_k$s. Since these RVs are independent and, according to assumption (ii), $\mathrm{E}\{|[\mathbf{f}]_k|^2\} = 1$, the expectation in (12) could be expressed as (13), shown at the top of the next page, where $z_k = \frac{r_k}{R}\sin\left(\frac{\phi_{p+1}+\phi_{q+1}+\theta_{l,p+1}+\theta_{l',q+1}}{2} - \psi_k\right)$ and $f_{z_k}(z)$ is its pdf. In order to compute the latter, one must have prior knowledge of the WSN nodes' distribution. Please note here that such information could be either easily integrated in nodes' memories prior to deployment or broadcasted by the receiver

$$\mathrm{E}_{r_k,\psi_k}\left\{ e^{-j\frac{4\pi R}{\lambda}\sin\left(\frac{\phi_{p+1}-\phi_{q+1}+\theta_{l,p+1}-\theta_{l',q+1}}{2}\right)\frac{r_k}{R}\sin\left(\frac{\phi_{p+1}+\phi_{q+1}+\theta_{l,p+1}+\theta_{l',q+1}}{2}-\psi_k\right)}\right\}$$
$$= \int_{-1}^{1} e^{-j\frac{4\pi R}{\lambda}\sin\left(\frac{\phi_{p+1}-\phi_{q+1}+\theta_{l,p+1}-\theta_{l',q+1}}{2}\right)z_k} f_{z_k}(z)dz, \quad (13)$$

$$\begin{aligned}[\mathbf{\Pi}]_{pq} &= \sum_{l,l'=1}^{L}\alpha_{l,p+1}\alpha^*_{l',q+1}\left(\sum_{p=0}^{+\infty}\frac{\left(4\pi\frac{R}{\lambda}\right)^p \sin^p\left(\frac{\phi_{p+1}-\phi_{q+1}+\theta_{l,p+1}-\theta_{l',q+1}}{2}\right)}{p!}(-j)^p\int_{-1}^{1} z_k^p\frac{2}{\pi}\sqrt{1-z^2}dz\right)\\ &= \sum_{l,l'=1}^{L}\alpha_{l,p+1}\alpha^*_{l',q+1}\left(\sum_{p=0}^{+\infty}\frac{\left(4\pi\frac{R}{\lambda}\right)^{2p}\sin^{2p}\left(\frac{\phi_{p+1}-\phi_{q+1}+\theta_{l,p+1}-\theta_{l',q+1}}{2}\right)(-1)^p}{2^{2p}p!(p+1)!}\right)\\ &= \sum_{l,l'=1}^{L}\alpha_{l,p+1}\alpha^*_{l',q+1}\Delta\left(\phi_{p+1}-\phi_{q+1}+\theta_{l,p+1}-\theta_{l',q+1}\right), \end{aligned} \quad (14)$$

at negligible overhead and power costs. Since the WSN nodes are uniformly distributed over a disc of radius R, one can easily show that $f_{z_k}(z) = \frac{2}{\pi}\sqrt{1-z^2}$, $z \in [-1, 1]$ [2]. Exploiting the power series expansion of the exponential function in (13), we obtain (14) as shown on the top of this page, where

$$\Delta(\phi) = 2\frac{J_1\left(4\pi\frac{R}{\lambda}\sin(\phi/2)\right)}{4\pi\frac{R}{\lambda}\sin(\phi/2)}. \quad (15)$$

Please note in the third line of (14) that we use the power series expansion of the Bessel function given by $J_n(x) = \sum_{p=0}^{+\infty}\frac{(-1)^p}{p!(n+p)!}\left(\frac{x}{2}\right)^{2p+n}$. It follows from (14) and (15) that $\mathbf{\Pi}$ depends solely on information locally available at every collaborating node and, hence, is locally computable. Following the above steps, one can also obtain for $p = 1, \ldots, M_I$

$$\begin{aligned}[\boldsymbol{\beta}]_p &= \lim_{K\to\infty}\frac{\left[\mathbf{H}_{\mathrm{I}}^H\mathbf{h}_1\right]_p}{K}\\ &= \sum_{l,l'=1}^{L}\alpha_{l,p+1}\alpha^*_{l',1}\Delta\left(\phi_{p+1}+\theta_{l,p+1}-\theta_{l',1}\right), \end{aligned} \quad (16)$$

and

$$\boldsymbol{\beta}_0 = \sum_{l,l'=1}^{L}\alpha_{l,1}\alpha^*_{l',1}\Delta\left(\theta_{l',1}-\theta_{l,1}\right). \quad (17)$$

As could be observed from (16) and (17), $\boldsymbol{\beta}$ and $\boldsymbol{\beta}_0$ are also independent of any information unavailable at every node, making them locally computable as well. Using (14), (16), and (17), we introduce our proposed DZFB vector

$$\mathbf{w}_{\mathrm{P}} = \frac{\left(\mathbf{h}_1 - \mathbf{H}_{\mathrm{I}}\mathbf{\Pi}^{-1}\boldsymbol{\beta}\right)}{K\left(\boldsymbol{\beta}_0 - \boldsymbol{\beta}^H\mathbf{\Pi}^{-1}\boldsymbol{\beta}\right)}. \quad (18)$$

If $\mathbf{w}_{\mathrm{P}}$ is implemented in lieu of $\mathbf{w}_{\mathrm{ZF}}$, the k-th node would require $[\mathbf{h}_1]_k$ and $[\mathbf{H}_{\mathrm{I}}]_{km}, m = 2, \ldots, M$ (i.e., its own channels) as well as $\boldsymbol{\beta}_0$, $\mathbf{\Pi}^{-1}$, and $\boldsymbol{\beta}$, in order to derive its corresponding beamforming weight

$$[\mathbf{w}_{\mathrm{P}}]_k = \frac{1}{K}\left([\mathbf{h}_1]_k - \sum_{m=1}^{M}[\mathbf{H}_{\mathrm{I}}]_{km}\left[\mathbf{\Pi}^{-1}\boldsymbol{\beta}\right]_m\right) \times\left(\boldsymbol{\beta}_0 - \sum_{m=1}^{M}\left[\boldsymbol{\beta}^H\right]_m\left[\mathbf{\Pi}^{-1}\boldsymbol{\beta}\right]_m\right)^{-1}. \quad (19)$$

According to (14)-(17), all these entities depend solely on information locally available and/or obtainable at the k-th node. Therefore, the computation of $[\mathbf{w}_{\mathrm{P}}]_k$ does not require any information exchange between nodes, thereby lending itself to a distributed implementation over WSNs, that is in sharp contrast to $[\mathbf{w}_{\mathrm{ZF}}]_k$ in (8). By substantially reducing the overhead, the new DZFB dramatically improves both WSN spectral and power efficiencies.

V. Achieved Beampattern Characteristics

In order to verify the efficiency of the proposed distributed DZFB and its compliance with the conditions (5) and (6), we analyze in this section the characteristics of its achieved beampattern. The latter is nothing but the received power at Rx from any source located at $\phi_\star$ and hence is defined for any AFB vector $\mathbf{w}$ as

$$P_{\mathbf{w}}(\phi_\star) = \left|\mathbf{w}^H\mathbf{h}_m\right|^2. \quad (20)$$

It follows from (20) that $P_{\mathbf{w}_{\mathrm{P}}}(\phi_\star)$ is a complex combination of several random variables, making its analysis a tedious task. In this work, we propose to study instead the behavior of the average beampattern $\bar{P}_{\mathbf{w}_{\mathrm{P}}}(\phi_\star) = \mathrm{E}_{r_k,\psi_k,[\mathbf{f}]_k}\left\{\left|\mathbf{w}_{\mathrm{P}}^H\mathbf{h}_m\right|^2\right\}$ where the expectation is taken over all nodes' forward channels and positions.

The main result of this section is given in the following theorem:

Theorem 1: For any given $p_m(\theta)$ and $\sigma_m,\ m = 1,\ldots,M$, $\bar{P}_{\mathbf{w}_{\mathrm{P}}}(\phi_\star)$ can be expressed as

$$\bar{P}_{\mathbf{w}_{\mathrm{P}}}(\phi_\star) = \left(\boldsymbol{\beta}_0 - \boldsymbol{\beta}^H \boldsymbol{\Pi}^{-1}\boldsymbol{\beta}\right)^{-2} \left(\frac{1}{K}\left(\Sigma_0(\phi_\star) - 2\mathrm{Re}\left(\boldsymbol{\Sigma}_2^H(\phi_\star)\boldsymbol{\Pi}^{-1}\boldsymbol{\beta}\right) + \boldsymbol{\beta}^H\boldsymbol{\Pi}^{-1}\boldsymbol{\Sigma}_3(\phi_\star)\boldsymbol{\Pi}^{-1}\boldsymbol{\beta}\right) + \left(1 - \frac{1}{K}\right)\left|\Sigma_1(\phi_\star) - \boldsymbol{\Sigma}_4^H(\phi_\star)\boldsymbol{\Pi}^{-1}\boldsymbol{\beta}\right|^2\right), \tag{21}$$

where the scalars Σ_0 and Σ_1 as well the vectors $\boldsymbol{\Sigma}_2$, $\boldsymbol{\Sigma}_3$, and $\boldsymbol{\Sigma}_4$ are complex functions of the sources' directions and their angular deviations.

Proof: See Appendix A.

It follows from (21) that the desired power $\bar{P}_{\mathbf{w}_{\mathrm{P}}}(\phi_1 = 0)$ boils down for large K to

$$\bar{P}_{\mathbf{w}_{\mathrm{P}}}(0) = \left(\frac{\left|\Sigma_1(0) - \boldsymbol{\Sigma}_4^H(0)\boldsymbol{\Pi}^{-1}\boldsymbol{\beta}\right|}{\left(\boldsymbol{\beta}_0 - \boldsymbol{\beta}^H\boldsymbol{\Pi}^{-1}\boldsymbol{\beta}\right)}\right)^2. \tag{22}$$

It can be inferred from the definitions of $\Sigma_1(\phi_m)$ and $\boldsymbol{\Sigma}_4(\phi_m)$ that they reduce for $\phi_m = \phi_1 = 0$ to $\boldsymbol{\beta}_0$ and $\boldsymbol{\beta}$, respectively. Consequently, from (22), $\bar{P}_{\mathbf{w}_{\mathrm{P}}}(0) = 1$ when K is large enough. This implies that the proposed DZFB guarantees a unit received power response at the desired direction, thereby satisfying at large K the condition in (5) as its conventional ZFB counterpart which is, however, unsuitable for a distributed implementation over WSNs. Simulations in Section VII will prove that $\bar{P}_{\mathbf{w}_{\mathrm{P}}}(0)$ exhibits for small K only a slight deterioration. Actually, this loss is nothing but the cost of adopting the asymptotic approximation at large K when designing $\mathbf{w}_{\mathrm{P}}$ in Section IV. Nevertheless, $\bar{P}_{\mathbf{w}_{\mathrm{P}}}(0)$ increases rapidly with K and reaches 1 for K in the range of 10.

Let us now derive the power received from the interfering sources. According to the definition of $\boldsymbol{\Sigma}_4^H(\phi_m)$ in Appendix A, we have for $m = 2,\ldots,M$

$$[\boldsymbol{\Sigma}_4(\phi_m)]_p = \sum_{l,l'=1}^{L} \alpha_{l,m}\alpha_{l',p+1}^* \Delta(\theta_{l,m} - \theta_{l',p+1} + \phi_m - \phi_{p+1}) = [\boldsymbol{\Pi}]_{(m-1)p}. \tag{23}$$

This implies that $\boldsymbol{\Sigma}_4(\phi_m) = e_m\boldsymbol{\Pi}$ where e_m is the vector having 1 in its m-th entry and zeros elsewhere. Exploiting this propriety, one can easily prove that

$$\Sigma_1(\phi_m) = \boldsymbol{\Sigma}_4^H(\phi_m)\boldsymbol{\Pi}^{-1}\boldsymbol{\beta}. \tag{24}$$

It follows from (21) and (24) that the m-th interference power is given by

$$\bar{P}_{\mathbf{w}_{\mathrm{P}}}(\phi_m) = \frac{1}{K\left(\boldsymbol{\beta}_0 - \boldsymbol{\beta}^H\boldsymbol{\Pi}^{-1}\boldsymbol{\beta}\right)^2}\left(\Sigma_0(\phi_m) - 2\mathrm{Re}\left(\boldsymbol{\Sigma}_2^H(\phi_m)\boldsymbol{\Pi}^{-1}\boldsymbol{\beta}\right) + \boldsymbol{\beta}^H\boldsymbol{\Pi}^{-1}\boldsymbol{\Sigma}_3(\phi_m)\boldsymbol{\Pi}^{-1}\boldsymbol{\beta}\right). \tag{25}$$

Despite its efficiency, our proposed technique does not totally suppress the interference sources, in contrast to conventional ZFB that can perfectly implement the condition (5) while being, however, unsuitable for a distributed implementation over WSNs. Actually, this is again the cost of adopting the asymptotic approximation approach introduced in Section IV when designing $\mathbf{w}_{\mathrm{P}}$. Nevertheless, according to (25), the proposed DZFB is able to linearly reduce the powers of all interfering sources by factor K and, hence, cancel them, when the number of collaborating nodes is large enough.

All these observations verify that the average beampattern achieved by the proposed DZFB has a main lobe peak at the desired source direction and $(M-1)$ minima at the interfering ones. As K grows large, the peak's and minima's values approach 1 and 0, respectively, thereby satisfying (5) and (6) as its ZFB counterpart which is, however, unsuitable for a distributed implementation over WSNs.

In the sequel, we compare the performance of our proposed technique with the existing distributed AFB benchmarks.

VI. Performance Comparison With Distributed AFB Benchmarks

So far, only two distributed AFB techniques exist: the monochromatic AFB $\mathbf{w}_{\mathrm{M}}$ which ignores scattering to assume a single-ray channel [2], [4], [8], [31] and the bichromatic AFB $\mathbf{w}_{\mathrm{B}}$ whose design relies on a polychromatic channel's approximation by two chromatics at $\pm\sigma_\theta$ when the latter is relatively small [22], [23]. It can be easily shown that $\mathbf{w}_{\mathrm{M}}$ is given by

$$\mathbf{w}_{\mathrm{M}} = \frac{\left(\mathbf{h}_{\mathrm{M},1} - \mathbf{H}_{\mathrm{M,I}}\boldsymbol{\Pi}_{\mathrm{M}}^{-1}\boldsymbol{\beta}_{\mathrm{M}}\right)}{K\left(1 - \boldsymbol{\beta}_{\mathrm{M}}^H\boldsymbol{\Pi}_{\mathrm{M}}^{-1}\boldsymbol{\beta}_{\mathrm{M}}\right)}, \tag{26}$$

where $\mathbf{h}_{\mathrm{M},m} = \mathbf{f}\odot\mathbf{g}_m^{(1)}$, $\mathbf{H}_{\mathrm{M,I}}^H = \left[\mathbf{f}\odot\mathbf{g}_2^{(1)}\ldots\odot\mathbf{g}_{\mathbf{M}}^{(\mathbf{1})}\right]$, $[\boldsymbol{\Pi}_{\mathrm{M}}]_{ij} = \Delta(\phi_{i+1} - \phi_{j+1})$, and $[\boldsymbol{\beta}_{\mathrm{M}}]_i = \Delta(\phi_{i+1})$. Whereas, $\mathbf{w}_{\mathrm{B}}$ is given by

$$\mathbf{w}_{\mathrm{B}} = \frac{\left(\mathbf{h}_{\mathrm{B},1} - \mathbf{H}_{\mathrm{B,I}}\boldsymbol{\Pi}_{\mathrm{B}}^{-1}\boldsymbol{\beta}_{\mathrm{B}}\right)}{K\left(1 + \Delta(2\sigma_\theta) - \boldsymbol{\beta}_{\mathrm{B}}^H\boldsymbol{\Pi}_{\mathrm{B}}^{-1}\boldsymbol{\beta}_{\mathrm{B}}\right)}, \tag{27}$$

where $\mathbf{h}_{\mathrm{B},m} = \mathbf{f}\odot\left(e^{-j(2\pi/\lambda)r_k\cos(\phi_m+\sigma_m-\psi_k)} + e^{-j(2\pi/\lambda)r_k\cos(\phi_m-\sigma_m-\psi_k)}\right)$, $\mathbf{H}_{\mathrm{B,I}}^H = [\mathbf{h}_{\mathrm{B},2}\ldots\mathbf{h}_{\mathrm{B},M}]$, $[\boldsymbol{\Pi}_{\mathrm{B}}]_{ij} = \Delta\left(\tilde{\phi}_{i+1} - \tilde{\phi}_{j+1}\right)$, and $[\boldsymbol{\beta}_{\mathrm{B}}]_i = \Delta\left(\tilde{\phi}_1 - \tilde{\phi}_{i+1}\right)$ with $\tilde{\phi}_i = \phi_{i/2} - \sigma_{i/2}$ if i is even and $\tilde{\phi}_i = \phi_{(i-1)/2+1} + \sigma_{(i-1)/2+1}$ if i is odd. It follows from (26) and (27) that both $\mathbf{w}_{\mathrm{M}}$ and $\mathbf{w}_{\mathrm{B}}$ depend on the information commonly available at each node and, hence, lend themselves to a distributed implementation over WSNs.

In order to compare our proposed distributed AFB with its monochromatic and bichromatic counterparts, we need a performance metric that captures each technique's compliance with the design conditions (5) and (6). For the sake of tractability, we propose in this paper to adopt the achieved average-signal-to-average-interference-plus-noise ratio (ASAINR) defined for any $\mathbf{w}$ as $\gamma_{\mathbf{w}} = \bar{P}_{\mathbf{w}}(0)/\left(\bar{P}_{\mathbf{w}}(\phi_{m\neq1}) + \bar{N}_{\mathbf{w}}\right)$ where $\bar{N}_{\mathbf{w}}$ is the average noise power incurred by $\mathbf{w}$. To this end, one should first derive the equations of the achieved average beampattern using $\mathbf{w}_{\mathrm{M}}$ and $\mathbf{w}_{\mathrm{B}}$. To do so, we introduce the following theorem:

Theorem 2: For any given $p_m(\theta)$ and $\sigma_m,\ m = 1,\ldots,M$, $\bar{P}_{\mathbf{w}_{\rm B}}(\phi_\star)$ can be expressed as

$$\bar{P}_{\mathbf{w}_{\rm B}}(\phi_\star)=\frac{\frac{2}{K}+\left(4\left(1-\frac{1}{K}\right)\frac{\Psi_{\rm B}(\phi_\star)}{\left(1+\Delta(2\sigma_1)-\boldsymbol{\beta}_{\rm B}^T\boldsymbol{\Pi}_{\rm B}^{-1}\boldsymbol{\beta}_{\rm B}\right)}\right)}{\left(1+\Delta(2\sigma_1)-\boldsymbol{\beta}_{\rm B}^T\boldsymbol{\Pi}_{\rm B}^{-1}\boldsymbol{\beta}_{\rm B}\right)}, \quad (28)$$

where

$$\Psi_{\rm B}(\phi_\star) = \int_{\Theta_\star}\frac{p_\star(\theta)}{2}\Bigg(\Delta(\phi_\star+\theta+\sigma_1)+\Delta(\phi_\star+\theta-\sigma_1) - 2\boldsymbol{\tau}_{\rm B}(\phi_\star+\theta)^T\boldsymbol{\Pi}_{\rm B}^{-1}\boldsymbol{\beta}_{\rm B}\Bigg)^2 d\theta, \quad (29)$$

with $[\boldsymbol{\tau}_{\rm B}(\theta)]_m = (1/2)\Delta(\theta-\tilde{\phi}_{m+2})$ if $\theta \neq \tilde{\phi}_{m+2}$ and $[\boldsymbol{\tau}_{\rm B}(\theta)]_m = 1/2$ otherwise, and $\Theta_\star$ is the span of the pdf $p_\star(\theta)$ over which the integral is calculated.[2]

In turn $\bar{P}_{\mathbf{w}_{\rm M}}(\phi_\star)$ is given by

$$\bar{P}_{\mathbf{w}_{\rm M}}(\phi_\star)=\frac{\frac{1}{K}+\left(4\left(1-\frac{1}{K}\right)\frac{\Psi_{\rm M}(\phi_\star)}{\left(1-2\boldsymbol{\beta}_{\rm M}^T\boldsymbol{\Pi}_{\rm M}^{-1}\boldsymbol{\beta}_{\rm M}\right)}\right)}{\left(1-2\boldsymbol{\beta}_{\rm M}^T\boldsymbol{\Pi}_{\rm M}^{-1}\boldsymbol{\beta}_{\rm M}\right)}, \quad (30)$$

where

$$\Psi_{\rm M}(\phi_\star)=\int_{\Theta_\star}p_\star(\theta)\Big(\Delta(\phi_\star+\theta)-2\boldsymbol{\tau}_{\rm M}(\phi_\star+\theta)^T\boldsymbol{\Pi}_{\rm B}^{-1}\boldsymbol{\beta}_{\rm B}\Big)^2 d\theta, \quad (31)$$

with $[\boldsymbol{\tau}_{\rm M}(\theta)]_m = (1/2)\Delta(\theta-\phi_{m+1})$.

Proof: See Appendix B.

A. DZFB Gains Against Bichromatic AFB

It follows from (21) and (28) that the ASAINR gain achieved by the proposed AFB over its bichromatic counterpart reduces for large K to

$$\zeta_{\rm B} = \frac{4\left(1+\Delta(2\sigma_1)-\boldsymbol{\beta}_{\rm B}^T\boldsymbol{\Pi}_{\rm B}^{-1}\boldsymbol{\beta}_{\rm B}\right)^2}{\Psi_{\rm B}(0)}, \quad (32)$$

where $\zeta_{\rm B} = \gamma_{\mathbf{w}_{\rm P}}/\gamma_{\mathbf{w}_{\rm B}}$. Exploiting the fact that $\Delta(x) \to 1$ when $x \to 0$, one can easily prove from (32) that $\gamma_{\mathbf{w}_{\rm P}} = \gamma_{\mathbf{w}_{\rm B}}$ if $\sigma_m = 0, m = 1,\ldots M$ (i.e., there is no scattering). This is hardly surprising since $\mathbf{w}_{\rm P}$ boils down to $\mathbf{w}_{\rm B}$ in such condition. On the other hand, when $\sigma_m,\ m = 2,\ldots,M$ are relatively small (i.e., in lightly- to moderately-scattered environments), it can be shown that $\Psi_{\rm B}(0) \simeq 1$ and $\boldsymbol{\beta}_{\rm B}^T\boldsymbol{\Pi}_{\rm B}^{-1}\boldsymbol{\beta}_{\rm B} \ll 1$ if all sources are sufficiently far apart by satisfying [2], [23]

$$\sin(\phi_m-\phi_n) \gg \frac{3\lambda}{16\pi}, \quad m \neq n. \quad (33)$$

Therefore, $\gamma_{\mathbf{w}_{\rm P}} \simeq \gamma_{\mathbf{w}_{\rm B}}$ in lightly- to moderately-scattered environments. This is expected since the bichromatic AFB is able in such environments to achieve the same optimal performance of DZFB. This is due to the validity of the bichromatic channel approximation up to an AS value of around 17 deg. Nevertheless, since $\Delta(x) \to 0$ when $x \to \inf$, $\gamma_{\mathbf{w}_{\rm P}} > \gamma_{\mathbf{w}_{\rm B}}$ when σ_ms grow large. Consequently, DZFB outperforms its bichromatic counterpart in highly-scattered environments. Its achieved ASAINR gain increases with σ_1 since $\Psi_{\rm B}(0)$ is a decreasing function of the latter.

[2]In the Gaussian and Uniform distribution cases, $\Theta_\star = [-\inf, +\inf]$ and $\Theta_\star = [-\sqrt{3}\sigma_\theta, +\sqrt{3}\sigma_\theta]$, respectively.

B. DZFB Gains Against Monochromatic AFB

From (21) and (28), we have for large K

$$\zeta_{\rm M} = \frac{4\left(1-\boldsymbol{\beta}_{\rm M}^T\boldsymbol{\Pi}_{\rm M}^{-1}\boldsymbol{\beta}_{\rm M}\right)^2}{\Psi_{\rm M}(0)}, \quad (34)$$

where $\zeta_{\rm M} = \gamma_{\mathbf{w}_{\rm P}}/\gamma_{\mathbf{w}_{\rm M}}$. When the sources are enough distant from each other to satisfy (33), the right hand side (RHS) of (34) reduces to $4\left(\int_{\Theta_\star}p_\star(\theta)\Delta(\theta)^2\, d\theta\right)^{-1}$. Assuming that the scattering distribution is Uniform over $[-\sqrt{3}\sigma_1, \sqrt{3}\sigma_1]$ (i.e., $p(\theta) = 1/2\sqrt{3}\sigma_1$), for small σ_1 we have

$$\begin{aligned}\zeta_{\rm M} &\simeq 8\sqrt{3}(\pi R)^2\sigma_1\left(\int_{-\sqrt{3}\sigma_1}^{\sqrt{3}\sigma_1}\left(\frac{J_1\left(2\pi\frac{R}{\lambda}\theta\right)}{\theta}\right)^2 d\theta\right)^{-1}\\ &\simeq 8\sqrt{3}\sigma_1\left(\int_0^1\frac{{}_2F_3\left(2,\frac{3}{2};2,2,3,-12\pi^2\left(\frac{R}{\lambda}\right)^2\sigma_\theta^2\theta\right)}{\sqrt{\theta}}d\theta\right)^{-1}\\ &\simeq {}_3F_4\left(\frac{1}{2},2,\frac{3}{2};\frac{3}{2},2,2,3,-12\pi^2\left(\frac{R}{\lambda}\right)^2\sigma_1^2\right)^{-1}, \end{aligned} \quad (35)$$

where ${}_3F_4\left(\frac{1}{2},2,\frac{3}{2};\frac{3}{2},2,2,3,-12\pi^2(R/\lambda)^2\ x^2\right)$ is the hypergeometric function. The latter DZFB decreases with x from its maximum value of 1 obtained at 0. This implies that $\gamma_{\mathbf{w}_{\rm P}} = \gamma_{\mathbf{w}_{\rm M}}$ if $\sigma_1 = 0$. This is expected from (18) and (26) since $\mathbf{w}_{\rm P} \to \mathbf{w}_{\rm M}$ when there is no scattering. On the other hand, it can be inferred from (35) that $\gamma_{\mathbf{w}_{\rm P}} > \gamma_{\mathbf{w}_{\rm M}}$ if $\sigma_1 \neq 0$. Therefore, DZFB outperforms its monochromatic vis-a-vis that completely ignores scattering. Besides, its achieved ASAINR gain against the latter increases not only with AS, but also with R/λ.

C. Insightfulness of the ASINR Metric

This section evaluates the perspicacity of the ASAINR as a metric for faithful and meaningful performance comparisons. To do so, the following theorem establishes a very useful asymptotic relationship between the ASAINR and the more common average SINR (ASINR) metric:

Theorem 3: For any $\mathbf{w} \in \{\mathbf{w}_{\rm P}, \mathbf{w}_{\rm B}, \mathbf{w}_{\rm M}\}$ and any given $p_m(\theta)$ and $\sigma_m,\ m = 1,\ldots,M$, we have

$$\lim_{K\to\infty}\tilde{\gamma}_{\mathbf{w}} = \lim_{K\to\infty}\gamma_{\mathbf{w}}, \quad (36)$$

where $\tilde{\gamma}_{\mathbf{w}}$ denotes the ASINR achieved using $\mathbf{w}$.

Proof: See Appendix C.

The above theorem states that the ASAINR and ASINR are asymptotically equivalent and, hence, we have also $\lim_{K\to\infty}\tilde{\zeta}_{\rm B} = \lim_{K\to\infty}\zeta_{\rm B}$ and $\lim_{K\to\infty}\tilde{\zeta}_{\rm M} = \lim_{K\to\infty}\zeta_{\rm M}$ where $\tilde{\zeta}_{\rm B}$ and $\tilde{\zeta}_{\rm M}$ are the ASINR gains of the proposed DZFB against the bichromatic and monochromatic AFBs. Consequently, for large K the proposed beamformer outperforms also its counterparts in terms of ASINRs well, more so at larger AS values as previously shown in Section VI.

VII. Simulation Results

This section verifies the efficiency of the proposed DZFB using computer simulations. All empirical average quantities are calculated over 10^6 random realizations of r_k, ψ_k, $[\mathbf{f}]_k$ for $k = 1, \ldots, K$ and $\alpha_{l,m}$, $\theta_{l,m}$ for $l = 1, \ldots, L_m$. In all simulations, all sources have the same unit power, $\sigma_n^2 = \sigma_v^2 = 1$, and $L_m = 6$. We also consider that all rays have equal power $1/L_m$ (i.e., $\mathrm{E}\left\{|\alpha_{l,m}|^2\right\} = 1/L_m$) and $\theta_{l,m}$s are uniformly distributed random variables with variance σ^2.

Fig. 2 displays the empirical and analytical (i.e., equation (21)) curves of the average beampattern $\bar{P}_{\mathbf{w}_{\mathrm{P}}}(\phi_\star)$ achieved by DZFB versus $\phi_\star$ for $\sigma = 35$ deg, $R/\lambda = 10$, and different values of K. We consider in Figs. 2(a) and 2(b) three and two interfering sources at $(\phi_2, \phi_3, \phi_4) = (2, 4, 7)$ deg and $(\phi_2, \phi_3) = (2, 5)$ deg, respectively. These figures confirm that the analytical (i.e., equation (21)) and empirical values of $\bar{P}_{\mathbf{w}_{\mathrm{P}}}(\phi_\star)$ match perfectly. They also show that the DZFB's average beampattern has a peak at the desired direction (i.e., $\phi = 0$) and minima at the interfering ones. Furthermore, we observe that $\bar{P}_{\mathbf{w}_{\mathrm{P}}}(0)$ loses a fraction of dB for small K. As discussed in Section V, this negligible loss results from the asymptotic approximation at large K assumed in the design of $\mathbf{w}_{\mathrm{P}}$. Nevertheless, according to Figs. 2(a) and 2(b), $\bar{P}_{\mathbf{w}_{\mathrm{P}}}(0)$ rapidly increases with K to reach 1 at no more than 10 WSN nodes, thereby satisfying the design condition in (6). Besides, DZFB satisfies also the condition in (5) for relatively large K as $\bar{P}_{\mathbf{w}_{\mathrm{P}}}(\phi_{m\neq 1})$ substantially decreases with K to reach -11 and -15 dB at 20 and 50, respectively. And the difference of 4 dB (i.e., log10(50/20)) confirms the linear decrease of interference powers with K as stated in Section V. The DZFB is clearly able to achieve the optimal performance of its conventional ZFB counterpart whose implementation requires, however, prohibitive overhead and power consumption that makes it unsuitable for distributed implementation over WSNs. All these observations corroborate the analytical results of Section V.

Fig. 3 plots the ASINR and ASAINR achieved by $\mathbf{w} \in \{\mathbf{w}_{\mathrm{P}}, \mathbf{w}_{\mathrm{B}}, \mathbf{w}_{\mathrm{M}}\}$ as well as the ASINR achieved by $\mathbf{w}_{\mathrm{ZF}}$ versus the AS σ for $R/\lambda = 10$ and $K = 20$. It shows that the empirical curves match perfectly their analytical counterparts (i.e., equations (21), (28), and (30)), thereby validating the derivations and observations made in Sections V and VI including Theorem 3. Beyond this key verification, we observe from this figure that the ASANR achieved by the monochromatic AFB starts deteriorating very quickly from optimal performance level as soon as σ increases from 0, making it very sensitive to scattering in interfered environments even if it is light. This is hardly-surprising since $\mathbf{w}_{\mathrm{M}}$ ignores it completely to assume instead a single-ray (i.e., monochromatic) channel that is far from capturing all its polychromatic channel components (especially at moderate or high scattering). Such a channel mismatch becomes even worst when σ increases. On the other hand, DZFB closely approaches the optimal ASINR achieved using $\mathbf{w}_{\mathrm{ZF}}$ at any scattering level. Whereas, $\mathbf{w}_{\mathrm{B}}$ approaches the same performance level of $\mathbf{w}_{\mathrm{P}}$ in lightly- to moderately-scattered environments when σ is relatively small. Nevertheless, in highly-scattered environments, its performance substantially deteriorates as the σ grows large (i.e., $\sigma \geq 20$ deg). This is hardly surprising since the bichromatic AFB design relies on a two-ray approximation of the polychromatic channel that is only valid at relatively small σ. In highly-scattered environments, the increasing mismatch between the nominal bichromatic channel and the true polychromatic one severely degrades performance.

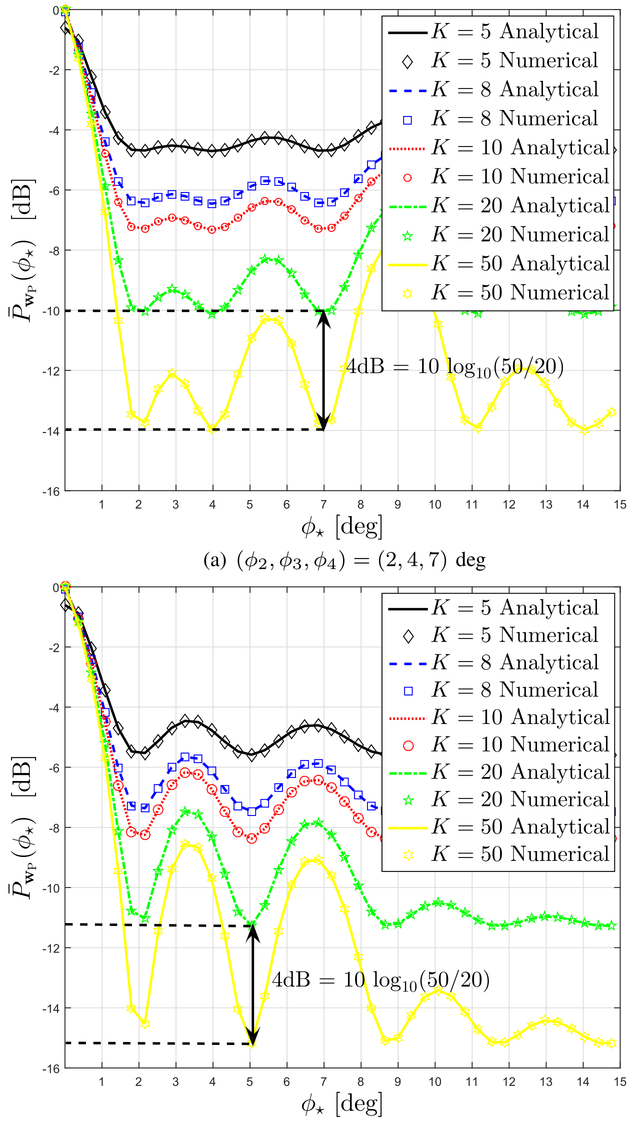

(a) $(\phi_2, \phi_3, \phi_4) = (2, 4, 7)$ deg

(b) $(\phi_2, \phi_3) = (2, 5)$ deg

Fig. 2. Empirical and analytical average beampattern $\bar{P}_{\mathbf{w}_{\mathrm{P}}}(\phi_\star)$ achieved by DZFB versus $\phi_\star$ for $\sigma = 35$ deg, $R/\lambda = 10$, $K = \{5, 8, 10, 20, 50\}$, and different sets of interfering sources.

Fig. 4 displays the ASINR and ASAINR gains achieved by the proposed DZFB against the conventional ZFB benchmark. As could be observed from this figure, for small K the proposed DZBF looses a fraction of dB that become more and more negligible as K increases. At $K = 20$, for instance, it losses 0.1461 dB which corresponds to as low as 3% loss with respect to the optimal performance achieved by the conventional ZFB. As discussed in Section V, this negligible loss results from the asymptotic approximation at large K

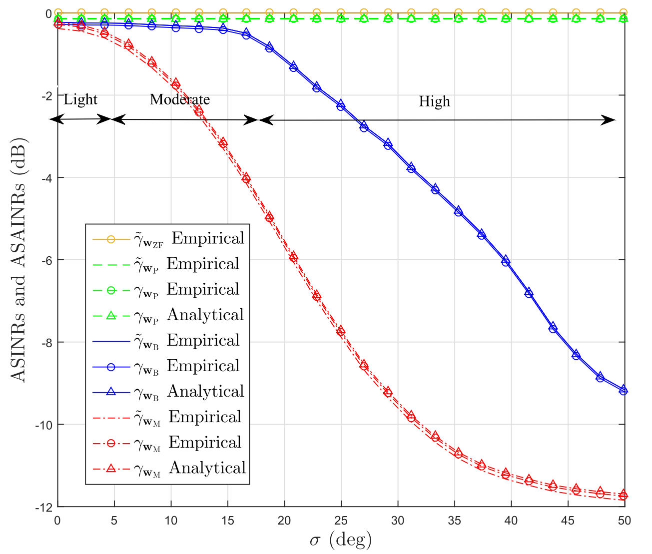

Fig. 3. Empirical ASINRs and ASAINRs achieved by the proposed DZFB and its monochromatic and bichromatic counterparts and their analytical ASAINRs versus σ for $R/\lambda = 10$ and $K = 20$.

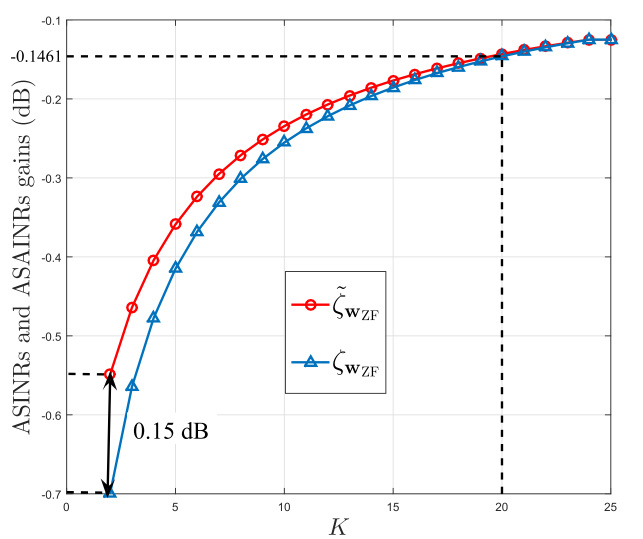

Fig. 4. ASINR and ASAINR gains of the proposed DZFB against its conventional ZBF counterpart versus K for $\sigma = 35$ deg and $R/\lambda = 10$.

assumed during the design of $\mathbf{w}_\mathrm{P}$ and, hence, it is the price to pay to make the proposed beamformer distributed. On the other hand, according to Fig 4, the ASINR and ASAINR gain curves are indistinguishable for $K \geq 18$ while exhibiting a small gap of 0.15 at $K = 2$. This confirms again the relevance of the ASINRs as performance metric and, hence, validates the results in Theorem 3.

Fig. 5 plots the ASINR and ASAINR gains achieved by the proposed DZFB against the monochromatic and bichromatic benchmarks versus σ deg for $K = 20$ and different values of $R/\lambda = \{10, 15\}$. We can check that $\tilde{\gamma}_{\mathbf{w}_\mathrm{P}} = \tilde{\gamma}_{\mathbf{w}_\mathrm{B}} = \tilde{\gamma}_{\mathbf{w}_\mathrm{M}}$ at $\sigma = 0$ (i.e., there is no scattering) where we have $\mathbf{w}_\mathrm{P} = \mathbf{w}_\mathrm{B} = \mathbf{w}_\mathrm{M}$. In lightly-scattered environments, however, the proposed distributed DZFB outperforms its monochromatic counterpart. The former achieves over the latter an important ASINR gain that increases with R/λ to reach up to 3 dB (i.e., $\tilde{\gamma}_{\mathbf{w}_\mathrm{P}} = 2\tilde{\gamma}_{\mathbf{w}_\mathrm{M}}$) for $R/\lambda = 15$. In moderately-

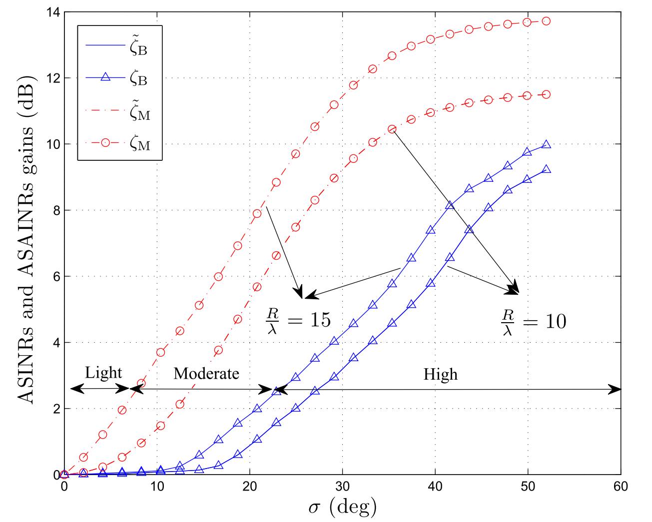

Fig. 5. ASINR and ASAINR gains of the proposed DZFB against its monochromatic and bichromatic benchmarks versus σ for $K = 20$ and different values of R/λ.

Qualitative Performance vs. Technique	Scattering Level in Interfered Environments		
	Light	Moderate	High
Monochromatic AFB	Low	Poor	Poor
Bichromatic AFB	Optimal	Optimal	Poor
Proposed DZFB	Optimal	Optimal	Optimal

Fig. 6. Qualitative performance of proposed DZFB and its distributed counterparts for different scattering levels in interfered environments.

scattered environments, ζ_M increases rapidly with σ, more so at higher R/λ, since $\mathbf{w}_\mathrm{M}$ is severely penalized by much larger channel mismatch. As far as the bichromatic AFB is concerned, $\zeta_\mathrm{B} = 1$ if $\sigma \leq 17$ deg. In moderately-scattered environments, its ASINR decreases slightly by 2 dB against DZFB at $\sigma = 20$ deg. In highly-scattered environments, DZFB unambiguously outperforms both its monochromatic and bichromatic counterparts by dramatic ASINR gains of up to 14 and 10 dB, respectively, thereby confirming its net superiority.

Table 6 qualitatively summarizes the performance of each distributed AFB technique at light, moderate, and high scattering levels in interfered environments. It demonstrates that DZFB is filling a large gap in the literature by extending the applicability range of distributed AFB to highly-scattered environments where none of its distributed predecessors was able to achieve acceptable performance.

Fig. 7 illustrates the existing trade-off for WSN AFBs between the channel mismatch level they incur and the amount of overhead and power consumptions they require in highly-scattered and interfered environments. In highly-scattered and interfered environments, only the proposed DZFB is able to reach the target trade-off zone (i.e., low mismatch and overhead & power consumptions). However, as σ decreases,

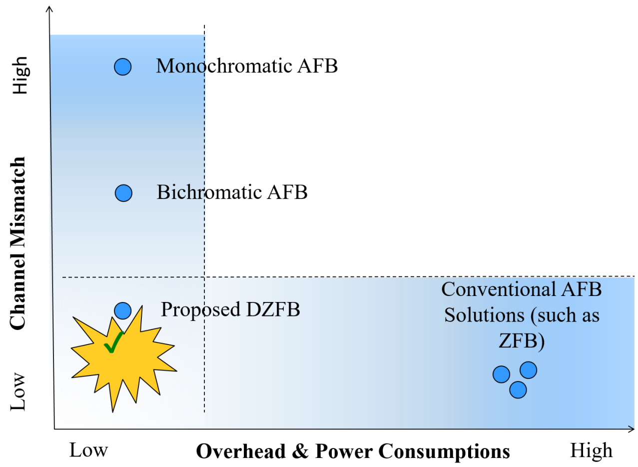

Fig. 7. Channel mismatch versus data exchange overhead and power consumption tradeoff in highly-scattered and interfered environments.

the bichromatic and monochromatic techniques move down towards the target zone. The bichromatic AFB would reach it first in moderately-scattered environments (i.e., $\sigma \leq 20$ deg) since the bichromatic channel approximation upon which it relies becomes then valid. In lightly-scattered environments (i.e., $\sigma \leq 10$ deg), the monochromatic AFB joins the proposed and bichromatic techniques at the target zone. Furthermore, if K decreases the proposed DZFB experiences a minor performance loss of a dB fraction when K decreases as shown in Section VII. Consequently, it moves up in Fig. 7 while staying in the target zone. However, when K increases, the proposed DZFB performance reaches optimality whereas the conventional ZFB sees it overhead and power costs increase dramatically thereby moving even further to the right of Fig. 7.

VIII. Conclusion

In this paper, OB was considered to establish a communication, through a WSN of K sensor nodes, from a source to a receiver in the presence of both scattering and interference. All sources send their data to the WSN during the first time slot while the nodes forward a properly weighted version of their received signals during the second slot. These ZFB weights are properly selected to maximize the desired power while completely canceling the interference signals. We showed that they depend on information locally unavailable at each node, making them unsuitable for WSNs from the prohibitive data exchange overhead and power depletion they would otherwise require. To address this issue, we exploit the asymptotic expression at large K of the ZFB weights that is locally computable at every node and, further, well-approximate their original counterparts. The performance of the resulting new DZFB version is analyzed and compared to ZFB and both monochromatic and bichromatic AFBs. We showed that DZFB is a best-of-two-words alternative for large σ that combines both advantages of its two counterparts (i.e., high performance and low overhead & power consumptions, respectively) while avoiding their weaknesses (i.e., low performance and high overhead & power consumptions, respectively).

Appendix A

The power received at Rx from the m-th source located at ϕ_m is defined as

$$\begin{aligned}\bar{P}_{\mathbf{w}_{\mathrm{P}}}(\phi_\star) &= \mathrm{E}\left\{\left|\mathbf{w}_{\mathrm{P}}^H(\mathbf{f}\odot\mathbf{g}_\star)\right|^2\right\}\\ &= \frac{1}{K^2\left(\boldsymbol{\beta}_0-\boldsymbol{\beta}^H\boldsymbol{\Pi}^{-1}\boldsymbol{\beta}\right)^2}\Big(\mathrm{E}\left\{\mathbf{h}_1^H\mathbf{h}_\star\mathbf{h}_\star^H\mathbf{h}_1\right\}\\ &\quad -\mathrm{E}\left\{\mathbf{h}_1^H\mathbf{h}_\star\mathbf{h}_\star^H\mathbf{H}_{\mathrm{I}}\boldsymbol{\Pi}^{-1}\boldsymbol{\beta}\right\}-\mathrm{E}\left\{\left(\mathbf{h}_1^H\mathbf{h}_\star\mathbf{h}_\star^H\mathbf{H}_{\mathrm{I}}\boldsymbol{\Pi}^{-1}\boldsymbol{\beta}\right)^*\right\}\\ &\quad +\mathrm{E}\left\{\left(\mathbf{H}_{\mathrm{I}}\boldsymbol{\Pi}^{-1}\boldsymbol{\beta}\right)^H\mathbf{h}_\star\mathbf{h}_\star^H\left(\mathbf{H}_{\mathrm{I}}\boldsymbol{\Pi}^{-1}\boldsymbol{\beta}\right)\right\}\Big)\\ &= \frac{\left(\mathrm{E}(\Gamma_1)-\mathrm{E}(\Gamma_2)-\mathrm{E}(\Gamma_2^*)+\mathrm{E}(\Gamma_3)\right)}{K^2\left(\boldsymbol{\beta}_0-\boldsymbol{\beta}^H\boldsymbol{\Pi}^{-1}\boldsymbol{\beta}\right)^2},\end{aligned} \tag{37}$$

where the expectation is taken over r_ks, ψ_ks, and $[\mathbf{f}]_k$s and $\Gamma_1 = \mathbf{h}_1^H\mathbf{h}_\star\mathbf{h}_\star^H\mathbf{h}_1$, $\Gamma_2 = \mathbf{h}_1^H\mathbf{h}_\star\mathbf{h}_\star^H\mathbf{H}_{\mathrm{I}}\boldsymbol{\Pi}^{-1}\boldsymbol{\beta}$, and $\Gamma_3 = \left(\mathbf{H}_{\mathrm{I}}\boldsymbol{\Pi}^{-1}\boldsymbol{\beta}\right)^H\mathbf{h}_\star\mathbf{h}_\star^H\mathbf{H}_{\mathrm{I}}\boldsymbol{\Pi}^{-1}\boldsymbol{\beta}$.

Let us first start by deriving the expression of Γ_1 as (38), as shown in the top of the next page. On the other hand, we have (39), shown also in the top of the next page, where $x = \sin\left((\phi_\star+\theta_{l,\star}-\theta_{l',1})/2\right)$, $x' = (\phi_\star+\theta_{l,\star}+\theta_{l',1})/2$, $y = \sin\left((\theta_{l_1,1}-\phi_\star-\theta_{l_2,\star})/2\right)$, and $y' = (\theta_{l_1,1}+\phi_\star+\theta_{l_2,\star})/2$. Exploiting the fact that r_ps and ψ_ps are mutually independent RV with pdfs

$$f_{r_p}(r) = \frac{2r}{R}, \quad 0 < r < R, \tag{40}$$

$$f_{\psi_p}(\psi) = \frac{1}{2\pi}, \quad -\pi \leq \psi < \pi, \tag{41}$$

respectively, we show that

$$\begin{aligned}&\mathrm{E}_{\psi_p}\left(e^{-j\frac{4\pi}{\lambda}r_p\left(x\sin\left(x'-\psi_p\right)+y\sin\left(y'-\psi_p\right)\right)}\right)\\ &\quad=\frac{1}{2\pi}\int_{-\pi}^{\pi}e^{-j\frac{4\pi}{\lambda}r_p\left(x\sin\left(x'-\psi_p\right)+y\sin\left(y'-\psi_p\right)\right)}d\psi_p\\ &\quad=I_0\left(-j\frac{4\pi}{\lambda}r_p\sqrt{x^2+y^2+2xy\cos(x'-y')}\right)\\ &\quad=J_0\left(\frac{4\pi}{\lambda}r_p\sqrt{x^2+y^2+2xy\cos(x'-y')}\right).\end{aligned} \tag{42}$$

By averaging this expression over r_p, we obtain

$$\begin{aligned}&\mathrm{E}_{r_p,\psi_p}\left(e^{j\frac{4\pi}{\lambda}r_p\left(x\sin\left(x'-\psi_p\right)+y\sin\left(y'-\psi_p\right)\right)}\right)\\ &=\mathrm{E}_{r_p}\left(J_0\left(\frac{4\pi}{\lambda}r_p\sqrt{x^2+y^2+2xy\cos(x'-y')}\right)\right)\\ &=\int_0^R\sum_{p=0}^{\infty}\frac{(-1)^p}{(p!)^2}\left(\frac{4\pi}{2\lambda}\right)^{2p}\sqrt{x^2+y^2+2xycos(x'-y')}^{2p}\\ &\quad\times(r_p)^{2p}\left(\frac{2r_p}{R}\right)dr_p\\ &=\sum_{p=0}^{\infty}\frac{(-1)^p}{p!(p+1)}\left(\frac{4\pi R\sqrt{x^2+y^2+2xy\cos(x'-y')}}{2\lambda}\right)^{2p}\\ &=\frac{2\lambda J_1\left(\frac{4\pi R}{\lambda}\sqrt{x^2+y^2+2xy\cos(x'-y')}\right)}{4\pi R\sqrt{x^2+y^2+2xy\cos(x'-y')}}\\ &=\Delta\left(\gamma_0\left(\phi_\star\right)\right),\end{aligned} \tag{43}$$

$$\Gamma_1 = \left(\sum_{p=1}^{K}\sum_{l,l'=1}^{L}\alpha_{l,\star}\alpha_{l',1}^{*}e^{-j\frac{2\pi}{\lambda}r_p\left[\cos(\phi_\star+\theta_{l,\star}-\psi_p)-\cos\left(\theta_{l',1}-\psi_p\right)\right]}\right) \times \left(\sum_{k=1}^{K}\sum_{l_1,l_2=1}^{L}\alpha_{l_1,1}\alpha_{l_2,\star}^{*}e^{-j\frac{2\pi}{\lambda}r_k\left[\cos\left(\theta_{l_1,1}-\psi_k\right)-\cos\left(\phi_\star+\theta_{l_2,\star}-\psi_k\right)\right]}\right)$$
$$= \sum_{p=1}^{K}\sum_{l,l',l_1,l_2=1}^{L}\alpha_{l,\star}\alpha_{l',1}^{*}\alpha_{l_1,1}\alpha_{l_2,\star}^{*}e^{-j\frac{2\pi}{\lambda}r_p\left[\cos(\phi_\star+\theta_{l,\star}-\psi_p)-\cos\left(\theta_{l',1}-\psi_p\right)+\cos\left(\theta_{l_1,1}-\psi_p\right)-\cos\left(\phi_\star+\theta_{l_2,\star}-\psi_p\right)\right]}$$
$$+\sum_{p=1}^{K}\sum_{k=1,k\neq p}^{K}\sum_{l,l',l_1,l_2=1}^{L}\alpha_{l,\star}\alpha_{l',1}^{*}\alpha_{l_1,1}\alpha_{l_2,\star}^{*}e^{-j\frac{2\pi}{\lambda}r_p\left[\cos(\phi_\star+\theta_{l,\star}-\psi_p)-\cos\left(\theta_{l',1}-\psi_p\right)\right]}e^{-j\frac{2\pi}{\lambda}r_k\left[\cos\left(\theta_{l_1,1}-\psi_k\right)-\cos\left(\phi_\star+\theta_{l_2,\star}-\psi_k\right)\right]}. \quad (38)$$

$$e^{-j\frac{4\pi}{\lambda}r_p\left(x\sin\left(x'-\psi_p\right)+y\sin\left(y'-\psi_p\right)\right)} = e^{-j\frac{2\pi}{\lambda}r_p\left[\cos(\phi_\star+\theta_l-\psi_p)-\cos(\theta_{l'}-\psi_p)\right]}e^{-j\frac{2\pi}{\lambda}r_p\left[\cos\left(\theta_{l_1}-\psi_p\right)-\cos\left(\phi_\star+\theta_{l_2}-\psi_p\right)\right]}, \quad (39)$$

where

$$\gamma_0(\phi_\star) = \arcsin\left(\left(x^2+y^2+2xy\cos(x'-y')\right)^{1/2}\right). \quad (44)$$

Using (43) in (38) yields

$$\mathrm{E}(\Gamma_1) = 2K\Sigma_0(\phi_\star)+4K(K-1)\Sigma_1(\phi_\star)\Sigma_1^*(\phi_\star), \quad (45)$$

where

$$\Sigma_0(\phi_\star) = \sum_{l,l',l_1,l_2=1}^{L}\alpha_{l,\star}\alpha_{l',1}^{*}\alpha_{l_1,1}\alpha_{l_2,\star}^{*}\Delta\left(2\gamma_0(\phi_\star)\right), \quad (46)$$

and

$$\Sigma_1(\phi_\star) = \sum_{l,l'=1}^{L}\alpha_{l,\star}\alpha_{l',1}^{*}\Delta\left(\theta_{l,\star}-\theta_{l',1}+\phi_\star\right). \quad (47)$$

Following the above approach, we can also obtain

$$\mathrm{E}(\Gamma_2) = 2K\boldsymbol{\Sigma}_2^H(\phi_\star)\boldsymbol{\Pi}^{-1}\boldsymbol{\beta}+4K(K-1)\Sigma_1(\phi_\star)\times\boldsymbol{\Sigma}_4^H(\phi_\star)\boldsymbol{\Pi}^{-1}\boldsymbol{\beta}, \quad (48)$$

where

$$[\boldsymbol{\Sigma}_2(\phi_\star)]_p = \sum_{l,l',l_1,l_2=1}^{L}\alpha_{l,\star}\alpha_{l',p+1}^{*}\alpha_{l_1,\star}\alpha_{l_2,p+1}^{*}\Delta(2\gamma_1(\theta,\phi_{p+1},\phi_\star)), \quad (49)$$

$\gamma_1(\phi_p,\phi_\star) = \arcsin\left(\left(x^2+y_1^2+2\,xy_1\cos(x'-y_1')\right)^{1/2}\right)$, $y_1 = \sin(\phi_p+\theta_{l_1,p}-\phi_\star-\theta_{l_2,\star})/2$, $y_1' = (\phi_p+\theta_{l_1,p}+\phi_\star+\theta_{l_2,\star})/2$, and $[\boldsymbol{\Sigma}_4(\phi_\star)]_p = \sum_{l,l'=1}^{L}\alpha_{l,\star}\alpha_{l',p+1}^{*}\Delta\left(\theta_{l,\star}-\theta_{l',p+1}+\phi_\star-\phi_{p+1}\right)$.
As far as $\mathrm{E}(\Gamma_3)$ is concerned, it can be expressed as

$$\mathrm{E}(\Gamma_3) = 2K\boldsymbol{\beta}^H\boldsymbol{\Pi}^{-1}\boldsymbol{\Sigma}_3(\phi_\star)\boldsymbol{\Pi}^{-1}\boldsymbol{\beta}+4K(K-1)\boldsymbol{\beta}^H\boldsymbol{\Pi}^{-1}\times\boldsymbol{\Sigma}_4(\phi_\star)\boldsymbol{\Sigma}_4^H(\phi_\star)\boldsymbol{\Pi}^{-1}\boldsymbol{\beta}, \quad (50)$$

where

$$[\boldsymbol{\Sigma}_3(\phi_\star)]_{pq} = \sum_{l,l',l_1,l_2=1}^{L}\alpha_{l,p+1}\alpha_{l',q+1}^{*}\alpha_{l_1,q+1}\alpha_{l_2,p+1}^{*}\times\Delta\left(2\gamma_2\left(\theta,\phi_{p+1},\phi_{q+1},\phi_\star\right)\right), \quad (51)$$

$\gamma_2(\phi_p,\phi_q,\phi_\star) = \arcsin\left(\left(x_1^2+y_1^2+2\,x_1y_1\cos(x_1'-y_1')\right)^{1/2}\right)$, $x_1 = \sin(\phi_\star+\theta_{l,p}-\phi_q-\theta_{l',q})/2$, $x_1' = (\phi_\star+\theta_{l,p}+\phi_q+\theta_{l',q})/2$, $y_1 = \sin\left(\phi_p+\theta_{l_1,q}-\phi_\star-\theta_{l_2,p}\right)/2$, and $y_1' = (\phi_p+\theta_{l_1,q}+\phi_\star+\theta_{l_2,p})/2$. Substituting (45), (48), and (50) in (37) yields to (21).

APPENDIX B

From (27), we have

$$\bar{P}_{\mathbf{w}_{\mathrm{B}}}(\phi_\star) = \frac{\mathrm{E}\{\eta_1\}-\mathrm{E}\{\eta_2\}-\mathrm{E}\{\eta_2^*\}+\mathrm{E}\{\eta_3\}}{K^2\left(1+\Delta(2\sigma_1)-\boldsymbol{\beta}_{\mathrm{B}}^T\boldsymbol{\Pi}^{-1}\boldsymbol{\beta}_{\mathrm{B}}\right)^2}, \quad (52)$$

where $\eta_1 = \boldsymbol{\beta}_{\mathrm{B}}^T\boldsymbol{\Pi}_{\mathrm{B}}^{-1}\mathbf{H}_{\mathrm{B,I}}^H\mathbf{h}_{\mathrm{B},m}\mathbf{h}_m^H\mathbf{H}_{\mathrm{B,I}}\boldsymbol{\Pi}_{\mathrm{B}}^{-1}\boldsymbol{\beta}_{\mathrm{B}}$, $\eta_2 = \mathbf{h}_{\mathrm{B},1}^H\mathbf{h}_{\mathrm{B},m}\mathbf{h}_m^H\mathbf{H}_{\mathrm{B,I}}\boldsymbol{\Pi}_{\mathrm{B}}^{-1}\boldsymbol{\beta}_{\mathrm{B}}$, and $\eta_3 = \mathbf{h}_{\mathrm{B},1}^H\mathbf{h}_{\mathrm{B},m}\mathbf{h}_m^H\mathbf{h}_{\mathrm{B},1}$.

Let us first focus on $\mathrm{E}\{\eta_3\}$. According to (i), we have

$$\mathrm{E}_{\alpha_{l,m}}\{\eta_1\} = \sum_{l=1}^{L}\frac{1}{L}\left(\boldsymbol{\beta}_{\mathrm{B}}^T\boldsymbol{\Pi}_{\mathrm{B}}^{-1}\mathbf{H}_{\mathrm{B,I}}^H\mathbf{g}_m^{(1)}(\phi_m+\theta_{l,m})\right)\times\left(\mathbf{g}_m^{(1)}(\phi_m+\theta_{l,m})^H\mathbf{H}_{\mathrm{B,I}}\boldsymbol{\Pi}_{\mathrm{B}}^{-1}\boldsymbol{\beta}_{\mathrm{B}}\right)$$
$$= \sum_{l=1}^{L}\frac{1}{L}\left(\sum_{p=1}^{2M-2}\left[\boldsymbol{\beta}_{\mathrm{B}}^T\boldsymbol{\Pi}_{\mathrm{B}}^{-1}\right]_p\left[\boldsymbol{\Pi}_{\mathrm{B}}^{-1}\boldsymbol{\beta}_{\mathrm{B}}\right]_p\varepsilon_p + \sum_{p=1}^{2M-2}\sum_{n=1,n\neq p}^{2M-2}\left[\boldsymbol{\beta}_{\mathrm{B}}^T\boldsymbol{\Pi}_{\mathrm{B}}^{-1}\right]_p\left[\boldsymbol{\Pi}_{\mathrm{B}}^{-1}\boldsymbol{\beta}_{\mathrm{B}}\right]_n\delta_{p,n}\right), \quad (53)$$

where $\varepsilon_p = \left[\mathbf{H}_{\mathrm{B,I}}^H\mathbf{g}_m^{(1)}(\phi_m+\theta_{l,m})\right]_p\left[\mathbf{g}_m^{(1)}(\phi_m+\theta_{l,m})^H\mathbf{H}_{\mathrm{B,I}}\right]_p$ and $\delta_{p,n} = \left[\mathbf{H}_{\mathrm{B,I}}^H\mathbf{g}_m^{(1)}(\phi_m+\theta_{l,m})\right]_p\left[\mathbf{g}_m^{(1)}(\phi_m+\theta_{l,m})^H\mathbf{H}_{\mathrm{B,I}}\right]_n$. ε_p could be equivalently rewritten as

$$\varepsilon_p = \left(\sum_{k=1}^{K}\left[\mathbf{H}_{\mathrm{B,I}}^H\right]_{pk}\left[\mathbf{g}_m^{(1)}(\phi_m+\theta_{l,m})\right]_k\right)\times\left(\sum_{s=1}^{K}\left[\mathbf{g}_m^{(1)}(\phi_m+\theta_{l,m})^H\right]_s[\mathbf{H}_{\mathrm{B,I}}]_{sp}\right)$$
$$= K+\sum_{k=1}^{K}e^{-j4\pi\frac{R}{\lambda}\sin\left(\frac{\phi_m+\theta_{l,m}-\tilde{\phi}_p}{2}\right)\sin\left(\psi_k-\frac{\phi_m+\theta_{l,m}+\tilde{\phi}_p}{2}\right)}\times\sum_{s=1,s\neq k}^{K}e^{j4\pi\frac{R}{\lambda}\sin\left(\frac{\phi_m+\theta_{l,m}-\tilde{\phi}_p}{2}\right)\sin\left(\psi_k-\frac{\phi_m+\theta_{l,m}+\tilde{\phi}_p}{2}\right)}. \quad (54)$$

Exploiting the fact that r_ks and ψ_ks are i.i.d random variables and $(2/\pi)\int_{-1}^{1} e^{j4\pi\frac{R}{\lambda}\sin\left(\frac{\phi}{2}\right)z}\sqrt{1-z^2}dz = \Delta(\phi)$, we show that

$$\mathrm{E}_{r_k,\psi_k}\{\varepsilon_p\} = K + 2K(K-1)\left[\boldsymbol{\tau}_{\mathrm{B}}(\phi_m+\theta_{l,m})\right]_p \times \left[\boldsymbol{\tau}_{\mathrm{B}}^T(\phi_m+\theta_{l,m})\right]_p. \quad (55)$$

We also show that

$$\mathrm{E}_{\alpha_{l,m},r_k,\psi_k}\{\delta_{p,n}\} = 2K(K-1)\left[\boldsymbol{\tau}_{\mathrm{B}}(\phi_m+\theta_{l,m})\right]_p \times \left[\boldsymbol{\tau}_{\mathrm{B}}^T(\phi_m+\theta_{l,m})\right]_n + 2K\left[\boldsymbol{\Pi}_{\mathrm{B}}\right]_{pq}. \quad (56)$$

It follows then from (55) and (56) that

$$\mathrm{E}_{\alpha_{l,m},r_k,\psi_k}\{\eta_1\} = \sum_{l=1}^{L}\frac{1}{L}\Big(2K\boldsymbol{\beta}_{\mathrm{B}}^T\boldsymbol{\Pi}_{\mathrm{B}}^{-1}\boldsymbol{\beta}_{\mathrm{B}} + 4K(K-1) \times \left(\boldsymbol{\tau}_{\mathrm{B}}^T(\phi_m+\theta_{l,m})\boldsymbol{\Pi}_{\mathrm{B}}^{-1}\boldsymbol{\beta}_{\mathrm{B}}\right)^2\Big), \quad (57)$$

since $[\boldsymbol{\Pi}_{\mathrm{B}}]_{pp} = 1/2$. Furthermore, following the same approach above, we prove that

$$\mathrm{E}_{\alpha_{l,m},r_k,\psi_k}\{\eta_2\} = \sum_{l=1}^{L}\frac{1}{L}\Bigg(2K\boldsymbol{\beta}_{\mathrm{B}}^T\boldsymbol{\Pi}_{\mathrm{B}}^{-1}\boldsymbol{\beta}_{\mathrm{B}} + 4K(K-1) \times \left(\frac{J_1(\gamma(\phi_m+\theta_{l,m}+\sigma_1))}{\gamma(\phi_m+\theta_{l,m}+\sigma_1)} + \frac{J_1(\gamma(\phi_m+\theta_{l,m}-\sigma_1))}{\gamma(\phi_m+\theta_{l,m}-\sigma_1)}\right) \times \boldsymbol{\tau}_{\mathrm{B}}^T(\phi_m+\theta_{l,m})\boldsymbol{\Pi}_{\mathrm{B}}^{-1}\Bigg), \quad (58)$$

and (59), as shown on the top of the next page. Note that $\mathrm{E}_{\alpha_{l,m},r_k,\psi_k}\{\eta_2\} = \mathrm{E}_{\alpha_{l,m},r_k,\psi_k}\{\eta_2^*\}$ since $\mathrm{E}_{r_k,\psi_k}\{\eta_2\}$ is real. Finally, applying the expectation with respect to $\theta_{l,m}$s over both sides of (57)-(59) and substituting the resulting equations in (52), $\bar{P}_{\mathbf{w}_{\mathrm{B}}}(\phi_\star)$ is obtained.

Now let us focus on $\bar{P}_{\mathbf{w}_{\mathrm{M}}}(\phi_\star)$. It can be observed from (26) and (27) that $\mathbf{w}_{\mathrm{B}}$ boils down, as expected, to $\mathbf{w}_{\mathrm{M}}$ when $\sigma_m = 0, m = 1, \ldots, M$ (i.e., there is no scattering). Therefore, by substituting σ_ms with 0 in (28), $\bar{P}_{\mathbf{w}_{\mathrm{M}}}(\phi_\star)$ is obtained as in (30).

APPENDIX C

In order to verify (36), one should derive $\mathrm{E}\{\lim_{K\to\infty} P_{\mathbf{w}_{\mathrm{P}}}\}$ and $\mathrm{E}\{\lim_{K\to\infty} N_{\mathbf{w}}\}$. Let us first focus on $\mathbf{w} = \mathbf{w}_{\mathrm{P}}$. From (37), we have

$$\mathrm{E}\left\{\lim_{K\to\infty} P_{\mathbf{w}_{\mathrm{P}}}(\phi_\star)\right\} = \frac{\mathrm{E}(\lim_{K\to\infty}\Gamma_1) - \mathrm{E}(\lim_{K\to\infty}\Gamma_2)}{K^2\left(\boldsymbol{\beta}_0 - \boldsymbol{\beta}^H\boldsymbol{\Pi}^{-1}\boldsymbol{\beta}\right)^2} - \frac{\mathrm{E}(\lim_{K\to\infty}\Gamma_2^*) - \mathrm{E}(\lim_{K\to\infty}\Gamma_3)}{K^2\left(\boldsymbol{\beta}_0 - \boldsymbol{\beta}^H\boldsymbol{\Pi}^{-1}\boldsymbol{\beta}\right)^2}. \quad (60)$$

It follows from (38) that we have (61), as shown on the top of the next page. Using the strong (39) along with LLN on the RHS of (61) yields

$$\lim_{K\to\infty}\Gamma_1 = \sum_{l,l',l_1,l_2=1}^{L}\alpha_{l,\star}\alpha_{l',1}^*\alpha_{l_1,1}\alpha_{l_2,\star}^* \times \left(\mathrm{E}\left\{e^{-j\frac{2\pi}{\lambda}r_p\left[\cos(\phi_\star+\theta_{l,\star}-\psi_p)-\cos\left(\theta_{l',1}-\psi_p\right)\right]}\right\} \times \mathrm{E}\left\{e^{-j\frac{2\pi}{\lambda}r_k\left[\cos\left(\theta_{l_1,1}-\psi_k\right)-\cos\left(\phi_\star+\theta_{l_2,\star}-\psi_k\right)\right]}\right\}\right) = 4\Sigma_1(\phi_\star)\Sigma_1^*(\phi_\star). \quad (62)$$

Following similar steps, we show

$$\lim_{K\to\infty}\Gamma_2 = 4\Sigma_1(\phi_\star)\boldsymbol{\Sigma}_4^H(\phi_\star)\boldsymbol{\Pi}^{-1}\boldsymbol{\beta}, \quad (63)$$

and

$$\lim_{K\to\infty}\Gamma_3 = 4\Sigma_1(\phi_\star)\boldsymbol{\Sigma}_4^H(\phi_\star)\boldsymbol{\Pi}^{-1}\boldsymbol{\beta}. \quad (64)$$

Furthermore, we have

$$N_{\mathbf{w}_{\mathrm{P}}} = \sigma_v^2\mathbf{w}_{\mathrm{P}}^H\boldsymbol{\Lambda}\mathbf{w}_{\mathrm{P}} + \sigma_n^2. \quad (65)$$

where $\boldsymbol{\Lambda} \triangleq \mathrm{diag}\{|[\mathbf{f}]_1|^2 \ldots |[\mathbf{f}]_K|^2\}$. Exploiting (14), (16), and (17), we can easily show that

$$\lim_{K\to\infty} N_{\mathbf{w}_{\mathrm{P}}} = \lim_{K\to\infty}\frac{\sigma_v^2}{K^2\left(\boldsymbol{\beta}_0 - \boldsymbol{\beta}^H\boldsymbol{\Pi}^{-1}\boldsymbol{\beta}\right)} + \sigma_n^2 = \sigma_n^2. \quad (66)$$

From (62)-(66), the asymptotic $\tilde{\gamma}_{\mathbf{w}_{\mathrm{P}}}$ can be expressed as

$$\lim_{K\to\infty}\tilde{\gamma}_{\mathbf{w}_{\mathrm{P}}} = \frac{1}{\sigma_n^2} = \lim_{K\to\infty}\tilde{\gamma}_{\mathbf{w}_{\mathrm{P}}}. \quad (67)$$

Let us now focus on $\mathbf{w} = \mathbf{w}_{\mathrm{B}}$. It is direct to show from (52) that

$$\mathrm{E}\left\{\lim_{K\to\infty} P_{\mathbf{w}_{\mathrm{B}}}(\phi_\star)\right\} = \frac{\mathrm{E}(\lim_{K\to\infty}\eta_1) - \mathrm{E}(\lim_{K\to\infty}\eta_2)}{K^2\left(1+\Delta(2\sigma_1) - \boldsymbol{\beta}_{\mathrm{B}}^T\boldsymbol{\Pi}^{-1}\boldsymbol{\beta}_{\mathrm{B}}\right)^2} - \frac{\mathrm{E}(\lim_{K\to\infty}\eta_2^*) - \mathrm{E}(\lim_{K\to\infty}\eta_3)}{K^2\left(1+\Delta(2\sigma_1) - \boldsymbol{\beta}_{\mathrm{B}}^T\boldsymbol{\Pi}^{-1}\boldsymbol{\beta}_{\mathrm{B}}\right)^2}. \quad (68)$$

It follows from the definition of η_1 that $\lim_{K\to\infty}\eta_1$ can be expressed as (69), as shown on the top of this page. Exploiting the strong LLN, one can prove that

$$\lim_{K\to\infty}\frac{1}{K}\mathbf{H}_{\mathrm{B,I}}^H\mathbf{g}_m^{(1)}(\phi) = 2\boldsymbol{\tau}_{\mathrm{B}}(\phi). \quad (70)$$

Substituting (70) in (69) and applying the expectation with respect to $\alpha_{l,m}$ over the resulting equation yields

$$\mathrm{E}_{\alpha_l}\left\{\lim_{K\to\infty}\eta_1\right\} = \frac{\sum_{l=1}^{L}\frac{4}{L}\left(\boldsymbol{\tau}_{\mathrm{B}}^T(\phi_m+\theta_{l,m})\boldsymbol{\Pi}_{\mathrm{B}}^{-1}\boldsymbol{\beta}_{\mathrm{B}}\right)^2}{\left(1+\Delta(2\sigma_1) - \boldsymbol{\beta}_{\mathrm{B}}^T\boldsymbol{\Pi}^{-1}\boldsymbol{\beta}_{\mathrm{B}}\right)^2}. \quad (71)$$

Please note that we exploit in (71) the fact that $\mathrm{E}\{\alpha_l\alpha_{l'}^*\} = 1$ if $l = l'$ and 0 otherwise, as stated in assumption (i). Following the same derivation steps above, it can be shown that

$$\mathrm{E}_{\alpha_{l,m},r_k,\psi_k}\left\{\eta_3\right\} = \sum_{l=1}^{L}\frac{2K\boldsymbol{\beta}_{\mathrm{B}}^T\boldsymbol{\Pi}_{\mathrm{B}}^{-1}\boldsymbol{\beta}_{\mathrm{B}} + 4K(K-1)\left(\frac{1}{L}\sum\frac{J_1(\gamma(\phi_m+\theta_{l,m}+\sigma_1))}{\gamma(\phi_m+\theta_{l,m}+\sigma_1)} + \frac{J_1(\gamma(\phi_m+\theta_{l,m}-\sigma_1))}{\gamma(\phi_m+\theta_{l,m}-\sigma_1)}\right)^2}{L}. \tag{59}$$

$$\begin{aligned}\lim_{K\to\infty}\Gamma_1 = \frac{1}{\left(\boldsymbol{\beta}_0 - \boldsymbol{\beta}^H\boldsymbol{\Pi}^{-1}\boldsymbol{\beta}\right)}&\Bigg(\left(\lim_{K\to\infty}\frac{1}{K}\right)\sum_{l,l',l_1,l_2=1}^{L}\alpha_{l,\star}\alpha_{l',1}^*\alpha_{l_1,1}\alpha_{l_2,\star}^*\\ &\times\lim_{K\to\infty}\sum_{p=1}^{K}\frac{1}{K}\times e^{-j\frac{2\pi}{\lambda}r_p\left[\cos(\phi_\star+\theta_{l,\star}-\psi_p)-\cos\left(\theta_{l',1}-\psi_p\right)+\cos\left(\theta_{l_1,1}-\psi_p\right)-\cos\left(\phi_\star+\theta_{l_2,\star}-\psi_p\right)\right]}\\ &+\left(\lim_{K\to\infty}\frac{K(K-1)}{K^2}\right)\sum_{l,l',l_1,l_2=1}^{L}\alpha_{l,\star}\alpha_{l,1'}^*\alpha_{l_1,1}\alpha_{l_2,\star}^*\lim_{K\to\infty}\frac{1}{K}\sum_{p=1}^{K}e^{-j\frac{2\pi}{\lambda}r_p\left[\cos(\phi_\star+\theta_{l,\star}-\psi_p)-\cos\left(\theta_{l',1}-\psi_p\right)\right]}\\ &\times\lim_{K\to\infty}\sum_{k=1,k\neq p}^{K}\frac{1}{(K-1)}e^{-j\frac{2\pi}{\lambda}r_k\left[\cos\left(\theta_{l_1,1}-\psi_k\right)-\cos\left(\phi_\star+\theta_{l_2,\star}-\psi_k\right)\right]}\Bigg).\end{aligned} \tag{61}$$

$$\lim_{K\to\infty}\eta_1 = \frac{\sum_{l,l'=1}^{L}\alpha_{l,\star}\alpha_{l',1}\left(\boldsymbol{\beta}_{\mathrm{B}}^T\boldsymbol{\Pi}_{\mathrm{B}}^{-1}\frac{\lim_{K\to\infty}\left(\mathbf{H}_{\mathrm{B,I}}^H\mathbf{g}_m^{(1)}(\phi_m+\theta_{l,m})\right)}{K}\right)\left(\lim_{K\to\infty}\frac{\left(\mathbf{g}_m^{(1)}\left(\phi_m+\theta_{l',1}\right)^H\mathbf{H}_{\mathrm{B,I}}\right)}{K}\boldsymbol{\Pi}_{\mathrm{B}}^{-1}\boldsymbol{\beta}_{\mathrm{B}}\right)}{\left(1+\Delta\left(2\sigma_1\right)-\boldsymbol{\beta}_{\mathrm{B}}^T\boldsymbol{\Pi}^{-1}\boldsymbol{\beta}_{\mathrm{B}}\right)^2}. \tag{69}$$

$$\begin{aligned}\mathrm{E}_{\alpha_l}\left\{\lim_{K\to\infty}\eta_2\right\} &= \frac{1}{\left(1+\Delta\left(2\sigma_1\right)-\boldsymbol{\beta}_{\mathrm{B}}^T\boldsymbol{\Pi}^{-1}\boldsymbol{\beta}_{\mathrm{B}}\right)^2}\\ &\times\sum_{l=1}^{L}\frac{8}{L}\Big(\Delta\left(\phi_m+\theta_{l,m}+\sigma_1\right)+\Delta\left(\phi_m+\theta_{l,m}-\sigma_1\right)\Big)\\ &\times\boldsymbol{\tau}_{\mathrm{B}}^T\left(\phi_m+\theta_{l,m}\right)\boldsymbol{\Pi}_{\mathrm{B}}^{-1},\end{aligned} \tag{72}$$

$$\mathrm{E}_{\alpha_l}\left\{\lim_{K\to\infty}\eta_3\right\} = \frac{1}{\left(1+\Delta\left(2\sigma_1\right)-\boldsymbol{\beta}_{\mathrm{B}}^T\boldsymbol{\Pi}^{-1}\boldsymbol{\beta}_{\mathrm{B}}\right)^2}$$

$$\times\sum_{l=1}^{L}\frac{4}{L}\Big(\Delta\left(\phi_m+\theta_{l,m}+\sigma_1\right)+\Delta\left(\phi_m\theta_{l,m}-\sigma_1\right)\Big)^2, \tag{73}$$

and

$$\mathrm{E}_{\alpha_l}\left\{\lim_{K\to\infty}N_{\mathbf{w}_{\mathrm{B}}}\right\} = \sigma_n^2. \tag{74}$$

Applying the expectation with respect to $\theta_{l,m}$ over (71)-(74) and using the resulting equations yields

$$\begin{aligned}\lim_{K\to\infty}\tilde{\gamma}_{\mathbf{w}_{\mathrm{B}}} &= \frac{\Psi_{\mathrm{B}}(0)}{4\left(1+\Delta\left(2\sigma_1\right)-\boldsymbol{\beta}_{\mathrm{B}}^T\boldsymbol{\Pi}_{\mathrm{B}}^{-1}\boldsymbol{\beta}_{\mathrm{B}}\right)^2}\\ &= \lim_{K\to\infty}\gamma_{\mathbf{w}_{\mathrm{B}}}.\end{aligned} \tag{75}$$

The same approach can be applied to show that

$$\begin{aligned}\lim_{K\to\infty}\tilde{\gamma}_{\mathbf{w}_{\mathrm{M}}} &= \frac{\Psi_{\mathrm{M}}(0)}{4\left(1-\boldsymbol{\beta}_{\mathrm{M}}^T\boldsymbol{\Pi}_{\mathrm{M}}^{-1}\boldsymbol{\beta}_{\mathrm{M}}\right)^2}\\ &= \lim_{K\to\infty}\gamma_{\mathbf{w}_{\mathrm{M}}}.\end{aligned} \tag{76}$$

REFERENCES

[1] S. Jayaprakasam, S. K. A. Rahim, and C. Y. Leow, "Distributed and collaborative beamforming in wireless sensor networks: Classifications, trends, and research directions," *IEEE Commun. Surveys Tuts.*, vol. 19, no. 4, pp. 2092–2116, 4th Quart., 2017.

[2] H. Ochiai, P. Mitran, H. V. Poor, and V. Tarokh, "Collaborative beamforming for distributed wireless ad hoc sensor networks," *IEEE Trans. Signal Process.*, vol. 53, no. 11, pp. 4110–4124, Nov. 2005.

[3] X. Shen, J. Huang, P. Liu, Y. Pan, B. Xu, and Z. Rao, "Analysis of collaborative beamforming for wireless sensor networks with phase offset," *Radioengineering*, vol. 23, no. 1, pp. 421–429, Apr. 2014.

[4] M. F. A. Ahmed and S. A. Vorobyov, "Collaborative beamforming for wireless sensor networks with Gaussian distributed sensor nodes," *IEEE Trans. Wireless Commun.*, vol. 8, no. 2, pp. 638–643, Feb. 2009.

[5] J. Huang, P. Wang, and Q. Wan, "Collaborative beamforming for wireless sensor networks with arbitrary distributed sensors," *IEEE Commun. Lett.*, vol. 16, no. 7, pp. 1118–1120, Jul. 2012.

[6] K. Zarifi, A. Ghrayeb, and S. Affes, "Distributed beamforming for wireless sensor networks with improved graph connectivity and energy efficiency," *IEEE Trans. Signal Process.*, vol. 58, no. 3, pp. 1904–1921, Mar. 2010.

[7] C. H. Wong, Z. W. Siew, M. K. Tan, R. K. Y. Chin, and K. T. K. Teo, "Optimization of distributed and collaborative beamforming in wireless sensor networks," in *Proc. IEEE CICSyN*, Phuket, Thailand, Jul. 2012, pp. 84–89.

[8] M. F. A. Ahmed and S. A. Vorobyov, "Sidelobe control in collaborative beamforming via node selection," *IEEE Trans. Signal Process.*, vol. 58, no. 12, pp. 6168–6180, Dec. 2010.

[9] R. Mudumbai, G. Barriac, and U. Madhow, "On the feasibility of distributed beamforming in wireless networks," *IEEE Trans. Wireless Commun.*, vol. 6, no. 5, pp. 1754–1763, May 2007.

[10] D. R. Brown, III, and H. V. Poor, "Time-slotted round-trip carrier synchronization for distributed beamforming," *IEEE Trans. Signal Process.*, vol. 56, no. 11, pp. 5630–5643, Nov. 2008.

[11] H. Ochiai, P. Mitran, H. V. Poor, and V. Tarokh, "Collaborative beamforming in ad hoc networks," in *Proc. IEEE ITW*, San Antonio, TX, USA, Oct. 2004, pp. 396–401.

[12] C. L. Godara, "Application of antenna arrays to mobile communications, Part II: Beam-forming and direction-of-arrival considerations," *Proc. IEEE*, vol. 85, no. 8, pp. 1195–1245, Aug. 1997.

[13] R. Mudumbai, D. R. Brown, III, U. Madhow, and H. V. Poor, "Distributed transmit beamforming: Challenges and recent progress," *IEEE Commun. Mag.*, vol. 47, no. 2, pp. 102–110, Feb. 2009.

[14] N. N. N. A. Malik, M. Esa, S. K. Yusof, and N. M. A. Latiff, "Collaborative beamforming null-steering array for wireless sensor networks," in *Proc. IEEE ISTT*, Langkawi, Malaysia, Nov. 2014, pp. 316–320.

[15] L. Dong, A. P. Petropulu, and H. V. Poor, "A cross-layer approach to collaborative beamforming for wireless ad hoc networks," *IEEE Trans. Signal Process.*, vol. 56, no. 7, pp. 2981–2993, Jul. 2008.

[16] D. Astely and B. Ottersten, "The effects of local scattering on direction of arrival estimation with MUSIC," *IEEE Trans. Signal Process.*, vol. 47, no. 12, pp. 3220–3234, Dec. 1999.

[17] O. Besson, P. Stoica, and A. B. Gershman, "Simple and accurate direction of arrival estimator in the case of imperfect spatial coherence," *IEEE Trans. Signal Process.*, vol. 49, no. 4, pp. 730–737, Apr. 2001.

[18] S. Shahbazpanahi, S. Valaee, and A. B. Gershman, “A covariance fitting approach to parametric localization of multiple incoherently distributed sources,” *IEEE Trans. Signal Process.*, vol. 52, no. 3, pp. 592–600, Mar. 2004.

[19] M. Souden, S. Affes, and J. Benesty, “A two-stage approach to estimate the angles of arrival and the angular spreads of locally scattered sources,” *IEEE Trans. Signal Process.*, vol. 56, no. 5, pp. 1968–1983, May 2008.

[20] M. Bengtsson and B. Ottersten, “Low-complexity estimators for distributed sources,” *IEEE Trans. Signal Process.*, vol. 48, no. 8, pp. 2185–2194, Aug. 2000.

[21] A. Amar, “The effect of local scattering on the gain and beamwidth of a collaborative beampattern for wireless sensor networks,” *IEEE Trans. Wireless Commun.*, vol. 9, no. 9, pp. 2730–2736, Sep. 2010.

[22] S. Zaidi and S. Affes, “Distributed collaborative beamforming in the presence of angular scattering,” *IEEE Trans. Commun.*, vol. 62, no. 5, pp. 1668–1680, May 2014.

[23] S. Zaidi and S. Affes, “Distributed collaborative beamforming design for maximized throughput in interfered and scattered environments,” *IEEE Trans. Commun.*, vol. 63, no. 12, pp. 4905–4919, Dec. 2015.

[24] S. Zaidi, O. B. Smida, S. Affes, and S. Valaee, “Energy-Efficient distributed amplify-and-forward beamforming for wireless sensor networks,” in *Proc. IEEE CAMSAP*, Curacao, Netherlands Antilles, Dec. 2017, pp. 1–5.

[25] H. Shen, W. Xu, S. Jin, and C. Zhao, “Joint transmit and receive beamforming for multiuser MIMO downlinks with channel uncertainty,” *IEEE Trans. Veh. Technol.*, vol. 63, no. 5, pp. 2319–2335, Jun. 2014.

[26] Z. Yi and I. M. Kim, “Joint optimization of relay-precoders and decoders with partial channel side information in cooperative networks,” *IEEE J. Sel. Areas Commun.*, vol. 25, no. 2, pp. 447–458, Feb. 2007.

[27] Y. Jing and H. Jafarkhani, “Network beamforming using relays with perfect channel information,” *IEEE Trans. Inf. Theory*, vol. 55, no. 6, pp. 2499–2517, Jun. 2009.

[28] H.-B. Kong, C. Song, H. Park, and I. Lee, “A new beamforming design for MIMO AF relaying systems with direct link,” *IEEE Trans. Commun.*, vol. 62, no. 7, pp. 2286–2295, Jul. 2014.

[29] S. Zaidi and S. Affes, “SNR and throughput analysis of distributed collaborative beamforming in locally-scattered environments,” *Wireless Commun. Mobile Comput.*, vol. 12, no. 18, pp. 1620–1633, Dec. 2012.

[30] M. Zeng, R. Zhang, and S. Cui, “On design of collaborative beamforming for two-way relay networks,” *IEEE Trans. Signal Process.*, vol. 59, no. 5, pp. 2284–2295, May 2011.

[31] K. Zarifi, S. Zaidi, S. Affes, and A. Ghrayeb, “A distributed amplify-and-forward beamforming technique in wireless sensor networks,” *IEEE Trans. Signal Process.*, vol. 59, no. 8, pp. 3657–3674, Aug. 2011.

[32] L. Dong, A. P. Petropulu, and H. V. Poor, “Weighted cross-layer cooperative beamforming for wireless networks,” *IEEE Trans. Signal Process.*, vol. 57, no. 8, pp. 3240–3252, Aug. 2009.

Slim Zaidi received the B.Eng. degree (Hons.) in telecommunications from the National Engineering School of Tunis, Tunis, Tunisia, in 2008, and the M.Sc. and Ph.D. degrees (Hons.) in electrical and computer engineering from INRS-EMT, Université du Québec, Montreal, QC, Canada, in 2011 and 2015, respectively. He is currently a Postdoctoral Fellow with the University of Toronto, Toronto, ON, Canada. He published over 50 peer-reviewed papers in major IEEE journals and conferences. His research interests include wireless systems (5G NR, LTE/LTE-A, LoRaWAN, NB-IoT, WSNs, and WiFi), radio access virtualization, machine learning and artificial intelligence, statistical signal and array processing, MIMO, cooperative communications, and millimeter wave communications. He received the National Grant of Excellence twice from the Tunisian Government for the M.Sc. (2009–2010) and Ph.D. (2011–2013) studies. He also received the Top-Tier Graduate Ph.D. Scholarships from the Natural Sciences and Engineering Research Council (NSERC) of Canada (2013–2015) and the Fonds de Recherche du Québec Nature et Technologies (FRQNT) (2013–2015). He also received two Prestigious Highly Selective Postdoctoral Fellowships from FRQNT (2016–2018) and NSERC (2017–2019). He also serves regularly as a TPC Member for top conferences (such as the IEEE PIMRC, the IEEE WCNC, and the IEEE GLOBECOM) and as a Reviewer for the IEEE TRANSACTIONS ON COMMUNICATIONS, the IEEE TRANSACTIONS ON WIRELESS COMMUNICATIONS, the IEEE ACCESS, and the IEEE WIRELESS COMMUNICATIONS LETTERS.

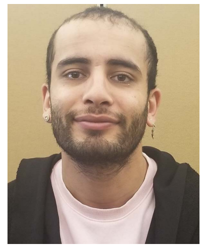

Oussama Ben Smida received the B.Eng. degree (Hons.) in telecommunications from the National Engineering School of Tunis, Tunis, Tunisia, in 2015, and the M.Sc. degree (Hons.) from the Centre Énergie Matériaux Télécommunications, Institut National de la Recherche Scientifique, Université du Québec, Montreal, QC, Canada, in 2017, where he is currently pursuing the Ph.D. degree. His research interests include collaborative beamforming, wireless ad hoc networks, and beyond 4G systems. He received the National Grant of Excellence twice from the Tunisian Government for the M.Sc. (2015–2017) and Ph.D. (since 2017) studies. He is also a Laureate of the scholarship of the INRS Academic Foundation Armand-Frappier for francophone students for the M.Sc. degree (2015).

Sofiène Affes (S’95–SM’05) received the Diplôme d’Ingénieur degree in telecommunications and the Ph.D. degree (Hons.) in signal processing from Télécom ParisTech (ENST), Paris, France, in 1992 and 1995, respectively. He was a Research Associate with INRS, Montreal, QC, Canada, until 1997, an Assistant Professor until 2000, and an Associate Professor until 2009. He is currently a Full Professor at INRS and the Director at INRS of PERWADE, a unique M$4 million research-training program on wireless in Canada involving 27 partners from eight universities and ten industrial organizations. He currently serves as a member of the Editorial Board of the *MDPI Sensors Journal* and the Advisory Board of the *MDPI Multidisciplinary Journal Science*. He was a recipient of the Discovery Accelerator Supplement Award twice from NSERC from 2008 to 2011 and from 2013 to 2016. In 2008 and 2015, he received the IEEE VTC Chair Recognition Award from the IEEE VTS and the IEEE ICUWB Chair Recognition Certificate from the IEEE MTT-S for exemplary contributions to the success of both the events. From 2003 to 2013, he was the Canada Research Chair in wireless communications. Since 2017, he has been the Cyrille-Duquet Research Chair in telecommunications. In 2006, 2015, and 2017, he served as the General Co-Chair or the Chair for the 64th IEEE VTC’2006-Fall, the 15th IEEE ICUWB’2015, and the 28th IEEE PIMRC’2017 jointly with co-located 28th IEEE 5G Summit, respectively, all held in Montreal, QC, Canada. He previously served as an Associate Editor for the IEEE TRANSACTIONS ON WIRELESS COMMUNICATIONS, the IEEE TRANSACTIONS ON COMMUNICATIONS, the IEEE TRANSACTIONS ON SIGNAL PROCESSING, the *Journal of Electrical and Computer Engineering* (Hindawi), and the *Journal of Wireless Communications and Mobile Computing* (Wiley).

Shahrokh Valaee was the Associate Chair of the Department for Undergraduate Studies from 2011 to 2017. He is the Founder and the Director of the Wireless and Internet Research Laboratory (WIRLab), University of Toronto, where he is also with the Edward S. Rogers Sr. Department of Electrical and Computer Engineering as a Professor. He is a fellow of the Engineering Institute of Canada. He was the TPC Co-Chair and the Local Organization Chair of the IEEE Personal Mobile Indoor Radio Communication (PIMRC) Symposium in 2011. He was the TCP Chair of PIMRC2017, the Track Co-Chair of WCNC 2014, and the TPC Co-Chair of ICT 2015. He has been a Guest Editor for various journals. From 2010 to 2012, he was an Associate Editor of the IEEE SIGNAL PROCESSING LETTERS. From 2010 to 2015, he served as an Editor for the IEEE TRANSACTIONS ON WIRELESS COMMUNICATIONS. He is currently an Editor of the *Journal of Computer and System Science*.